

# Coarray Tensor Completion for DOA Estimation

**Hang Zheng**, Student Member, IEEE  
Zhejiang University, Hangzhou, China

**Zhiguo Shi**, Senior Member, IEEE  
Zhejiang University, Hangzhou, China

**Chengwei Zhou**, Member, IEEE  
Zhejiang University, Hangzhou, China

**André L. F. de Almeida**, Senior Member, IEEE  
Federal University of Ceará, Fortaleza, Brazil

**Abstract**— Sparse array direction-of-arrival (DOA) estimation using tensor model has been developed to handle multi-dimensional sub-Nyquist sampled signals. Furthermore, augmented virtual arrays can be derived for Nyquist-matched coarray tensor processing. However, the partially augmentable sparse array corresponds to a discontinuous virtual array, whereas the existing methods can only utilize its continuous part. Conventional virtual linear array interpolation techniques complete coarray covariance matrices with dispersed missing elements, but fail to complete the coarray tensor with whole missing slices. In this paper, we propose a coarray tensor completion algorithm for two-dimensional DOA estimation, where the coarray tensor statistics can be entirely exploited. In particular, in order to impose an effective low-rank regularization on the slice-missing coarray tensor, we propose shift dimensional augmenting and coarray tensor reshaping approaches to reformulate a structured coarray tensor with sufficiently dispersed missing elements. Furthermore, the shape of the reformulated coarray

Part of this work was presented at IEEE International Conference on Acoustics, Speech and Signal Processing, Singapore, May 22-27, 2022 [1].

The work of H. Zheng, Z. Shi and C. Zhou was supported in part by the National Natural Science Foundation of China under Grants 62271444, U21A20456, and 61901413, the Zhejiang Provincial Natural Science Foundation of China under Grant LZ23F010007, the Zhejiang University Education Foundation Qizhen Scholar Foundation, and the 5G Open Laboratory of Hangzhou Future Sci-Tech City.

H. Zheng is with the College of Information Science and Electronic Engineering, Zhejiang University, Hangzhou 310027, China (e-mail: hangzheng@zju.edu.cn). Z. Shi is with the College of Information Science and Electronic Engineering, Zhejiang University, Hangzhou 310027, China, and also with the International Joint Innovation Center, Zhejiang University, Haining 314400, China (e-mail: shizg@zju.edu.cn). C. Zhou is with the College of Information Science and Electronic Engineering, Zhejiang University, Hangzhou 310027, China, and also with the Key Laboratory of Collaborative Sensing and Autonomous Unmanned Systems of Zhejiang Province, Hangzhou 310015, China (e-mail: zhouchw@zju.edu.cn). A. L. F. de Almeida is with the Department of Teleinformatics Engineering, Federal University of Ceará, Fortaleza 60020-181, Brazil (e-mail: andre@gtel.ufc.br). (*Corresponding author: Zhiguo Shi*)

0018-9251 © 2022 IEEE

tensor is optimized by maximizing the dispersion-to-percentage ratio of missing elements. As such, a coarray tensor nuclear norm minimization problem can be designed to optimize the completed coarray tensor corresponding to a filled virtual array, based on which the closed-form DOA estimation is achieved. Meanwhile, the global convergence of the coarray tensor completion is theoretically proved. Simulation results demonstrate the effectiveness of the proposed algorithm compared to other matrix-based and tensor-based methods.

**Index Terms**— Coarray tensor, direction-of-arrival estimation, sparse array, tensor completion.

## I. Introduction

**D**IRECTION-OF-ARRIVAL (DOA) estimation using sensor arrays has been intensively studied in the field of radar, sonar, speech, wireless communications, and so on [2–6]. Different from uniform arrays, sparse arrays including coprime arrays [7], nested arrays [8, 9], and others with optimized configurations [10] estimate DOAs of signals at sub-Nyquist sampling rate, which helps to alleviate antenna coupling and system overload [11]. In general, augmented virtual arrays can be derived from the second-order signal statistics of sparse arrays for Nyquist-matched coarray processing [12–14]. The common coarray-based DOA estimation methods include coarray Multiple Signal Classification (MUSIC) [15, 16], coarray Estimation of Signal Parameters via Rotational Invariance Technique (ESPRIT) [17], and coarray sparsity methods [18, 19], etc. They all follow the same principle of matrix-based signal processing, i.e., representing the received signals as a matrix, then flattening its second-order coarray statistics into a vector. However, with the increasing sparse array dimension, these methods fail to preserve the structure of multi-dimensional sub-Nyquist signals.

As an extension of matrix in the high-dimensional space, tensor has been utilized for multi-dimensional array processing, among which tensor decompositions [20] can estimate underlying multiway parameters in wireless communication and radar systems [21]. In particular, the Vandermonde structure constrained tensor decomposition method [22] and the Hermitian Toeplitz constrained tensor reconstruction method [23] have been respectively proposed to achieve two-dimensional (2-D) DOA estimation for transmit beamspace multiple-input multiple-output radar and coherent sources DOA estimation for uniform rectangular array. By incorporating tensor model with sub-Nyquist sampling, a tensor-based sub-Nyquist radar equipped with a thinned array was proposed for DOA estimation [24], where the first-order sub-Nyquist tensor signals were recovered via tensorial compressed sensing. More recently, augmented multi-dimensional virtual arrays were derived for coarray tensor DOA estimation [25, 26], which pushed the sub-Nyquist tensor model to the coarray domain. However, for partially augmentable sparse arrays such as the representative coprime array, the corresponding multi-dimensional discontinuous virtual arrays have slices of holes [27], resulting whole slices

of missing elements in the coarray tensor. The existing coarray tensor DOA estimation methods for partially augmentable sparse arrays have to discard discontinuous virtual sensors to extract a virtual uniform array. As such, they cannot utilize the entire coarray tensor statistics, and the resulting aperture reduction and resolution degradation cannot be compensated by tensor processing. Thus, we aim to make full use of the derived virtual array to enhance the estimation performance.

To fully utilize the entire coarray information, virtual array interpolation techniques have been proposed for DOA estimation with coprime linear arrays, among which matrix completion and matrix reconstruction are two mainstream solutions [28, 29]. In particular, matrix completion has been adopted to recover randomly missing elements in corrupted data matrix by imposing a low-rank regularization, which is normally relaxed to nuclear norm minimization. In order to complete the incomplete coarray covariance matrix corresponding to a discontinuous virtual linear array, a nuclear norm minimization optimization approach was proposed to yield an interpolated virtual linear array [28]. On the other hand, in order for gridless DOA estimation, the complete coarray covariance matrix corresponding to an interpolated virtual linear array was reconstructed via atomic norm minimization [29], where the Toeplitz property was utilized as a prior. Nevertheless, these virtual linear array interpolation techniques are only suitable for incomplete matrices with dispersed missing elements, but not for completing the coarray tensor with whole missing slices.

Due to the fact that adjacent missing elements in an incomplete tensor present a strong relevance, a low-rank regularization-based tensor completion technique was proposed to complete the randomly missing elements [30]. Since image data is normally corrupted by randomly missing pixels, the low-rank tensor completion technique has been applied to repair images [31]. However, the whole missing slices prevent a sufficient low-rank regularization on the coarray tensor. To recover regularly damaged images with slices of missing pixels, embedding space-based slice completion methods have gained many interests, where the Tucker or tensor train representation of the incomplete image tensor is approximated through an iterative rank increment procedure [32, 33]. Nevertheless, neither the Tucker rank nor the tensor train rank increment operation matches the canonical polyadic (CP) model of the coarray tensor, which means that the existing slice completion methods for image restoration are not applicable to coarray tensor completion. More recently, a CP approximation-based tensor completion method has been proposed to reconstruct the functional magnetic resonance imaging (fMRI) data with regular sub-Nyquist sampling patterns including both missing fibers and missing slices [34]. However, the fMRI tensor reconstruction modifies observed elements in the incomplete tensor, whereas the observed elements in the coarray tensor are expected to be preserved for DOA estimation. Thus, it remains challenging to effectively complete the slice-missing coarray

tensor for DOA estimation. To the best of our knowledge, it has not been addressed in the literature.

In this paper, we propose a 2-D sparse array DOA estimation algorithm based on coarray tensor completion. First, an incomplete coarray tensor corresponding to an augmented discontinuous virtual cubic array is derived from the sub-Nyquist tensor statistics. Due to the existence of whole missing slices in the coarray tensor, the conventional low-rank tensor completion techniques become ineffective. To address this issue, we reformulate the initial coarray tensor as a structured one with dispersed missing elements through shift dimensional augmenting and coarray tensor reshaping. Moreover, the shape of the reformulated coarray tensor is optimized by simultaneously maximizing the dispersion level of missing elements and minimizing the percentage of missing elements. As such, the reformulated coarray tensor can be successfully completed by solving a coarray tensor nuclear norm minimization problem via an alternating direction method of multipliers (ADMM). Meanwhile, we prove the global convergence of using the ADMM for coarray tensor completion. Finally, the completed coarray tensor corresponding to a filled virtual cubic array is decomposed to obtain the closed-form solution of azimuth and elevation angles. According to our numerical simulation results, the proposed coarray tensor completion algorithm is superior to conventional matrix-based and tensor-based methods in terms of estimation accuracy and angular resolution, and can simultaneously deal with uncorrelated and fully correlated signals.

In our previous work on sparse array DOA estimation [27], the continuous part of the multi-dimensional discontinuous virtual array was extracted for coarray tensor processing, whereas the problem of completing slice-missing coarray tensor has not been investigated. In this paper, however, we focus on the utilization of the entire coarray tensor statistics to further enhance the estimation performance. Regarding the problem of coherent sources DOA estimation in multi-path environments, we developed a tensor decorrelation method for uniform arrays [23], which does not consider the sub-Nyquist sampling scenario. In contrast, the effectiveness of coarray tensor processing for coherent sources estimation with sparse arrays is validated in this paper. Preliminary results of this work were presented in our conference paper [1]. In this paper, we will further investigate the optimal structure of the reformulated coarray tensor by designing a coarray sub-tensor size optimization problem, and present detailed derivations for the coarray tensor completion problem. Moreover, we will also provide theoretical analyses on the dispersion level of missing elements in the reformulated coarray tensor, global convergence of coarray tensor completion, and computational complexity.

The rest of the paper is organized as follows. In Section II, we present a tensor signal model for sparse array. In Section III, we reformulate the incomplete coarray tensor to distribute its missing elements, and in Section IV, we propose a coarray tensor completion method for DOA

estimation. We discuss the simulation results in Section V and make our conclusions in Section VI.

Notations of this paper are listed in TABLE I.

TABLE I  
LIST OF NOTATION

Symbol	Description
$a, \mathbf{a}, \mathbf{A}, \mathcal{A}$	Scalar, vector, matrix, and tensor
$j$	Imaginary unit
$\mathbb{C}, \mathbb{N}$	Complex number and natural number sets
$(\cdot)^T, (\cdot)^H, (\cdot)^*, (\cdot)^\dagger$	Transpose, Hermitian transpose, conjugation, and pseudoinverse
$[\cdot]_{(j)}$	Mode- $j$ tensor unfolding
$\text{o}(\cdot)$	Order of a tensor
$\times_j$	Mode- $j$ tensor-matrix product
$\mathcal{A}_1 \underset{j_1}{\times} \underset{j_2}{\mathcal{A}_2}$	Tensor contraction along the $j_1$ -th dimension of $\mathcal{A}_1$ and the $j_2$ -th dimension of $\mathcal{A}_2$
$[\cdot]_{\sqcup_j}$	Concatenation in the $j$ -th dimension
$\langle \cdot, \cdot \rangle$	Inner product between two tensors
$\mathbb{E}\{\cdot\}$	Statistical expectation
$\text{P}_\Omega(\mathcal{A})$	Projection of the elements in $\mathcal{A}$ onto the index set $\Omega$
$\circ, \otimes, \odot, \otimes$	Outer product, Kronecker product, Khatri-Rao product, and Hadamard product
$\ \cdot\ _F, \ \cdot\ _2, \ \cdot\ _*$	Frobenius norm, Euclidean norm, and nuclear norm
$\text{mod}(a, b)$	Modulo between $a$ and $b$
$\lfloor \cdot \rfloor$	Rounding down
$ \cdot $	Cardinality of a set or absolute value
$\angle$	Phase of a complex number
$\mathbf{I}, \mathcal{I}$	Identity matrix and identity tensor
$\mathbf{0}, \mathcal{O}$	Zero matrix and zero tensor

## II. Tensor Signal Model for Coprime Planar Array

In this paper, we adopt the coprime planar array, a typical partially augmentable sparse array, for DOA estimation. As shown in Fig. 1, the coprime planar array consists of two sparse uniform rectangular arrays (URAs)  $\{\mathbb{P}_i, i = 1, 2\}$ , where the sparse URA  $\mathbb{P}_i$  contains  $M_{\mathbb{P}_i}$  sensors along the  $x$ -axis and  $N_{\mathbb{P}_i}$  sensors along the  $y$ -axis, respectively. Specifically, we have  $M_{\mathbb{P}_1} = 2M_1$ ,  $N_{\mathbb{P}_1} = 2N_1$ , and  $M_{\mathbb{P}_2} = M_2$ ,  $N_{\mathbb{P}_2} = N_2$ , where  $M_1$  and  $M_2$  are coprime integers, as well as the pair of  $N_1$  and  $N_2$ . For sparse URA  $\mathbb{P}_1$ , its inter-element spacings along the  $x$ -axis and the  $y$ -axis are respectively  $d_{x_1} = M_2d$  and  $d_{y_1} = N_2d$ , where  $d = \lambda/2$  with  $\lambda$  being the signal wavelength. Similarly, the inter-element spacings along the  $x$ -axis and the  $y$ -axis for sparse URA  $\mathbb{P}_2$  are  $d_{x_2} = M_1d$  and  $d_{y_2} = N_1d$ , respectively. As such, the sensors of the coprime planar array are located at

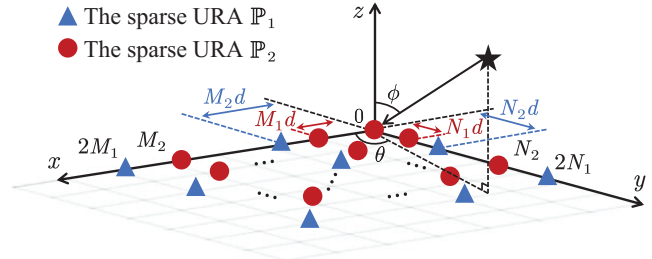


Fig. 1. The geometry of the coprime planar array.

$\{(x_{\mathbb{P}_1}, y_{\mathbb{P}_1}) \cup (x_{\mathbb{P}_2}, y_{\mathbb{P}_2}) \mid x_{\mathbb{P}_1} = d_{x_1}m_1, y_{\mathbb{P}_1} = d_{y_1}n_1, x_{\mathbb{P}_2} = d_{x_2}m_2, y_{\mathbb{P}_2} = d_{y_2}n_2\}$ , where  $m_1 \in \{0, 1, \dots, M_{\mathbb{P}_1} - 1\}$ ,  $n_1 \in \{0, 1, \dots, N_{\mathbb{P}_1} - 1\}$ ,  $m_2 \in \{0, 1, \dots, M_{\mathbb{P}_2} - 1\}$ , and  $n_2 \in \{0, 1, \dots, N_{\mathbb{P}_2} - 1\}$ . Note that, sparse URAs  $\mathbb{P}_1$  and  $\mathbb{P}_2$  only overlap at the origin  $(0, 0)$  due to their coprime deployment. Hence, there are total  $M_{\mathbb{P}_1}N_{\mathbb{P}_1} + M_{\mathbb{P}_2}N_{\mathbb{P}_2} - 1$  sensors in the deployed coprime planar array.

Assume that  $K$  uncorrelated far-field narrowband source signals impinge on the coprime planar array from directions  $\{(\theta_k, \phi_k), k = 1, 2, \dots, K\}$ , where  $\theta_k \in [0, \pi]$  and  $\phi_k \in [-\pi/2, \pi/2]$  are the azimuth and elevation of the  $k$ -th source, respectively. Under deployment of the planar array for 2-D DOA estimation, the array received signals are naturally embedded with the 2-D spatial information of the sources. However, the conventional signal model in a form of matrix only reflects the spatial information along a single dimension, causing the damage of structural signal characteristics. To overcome this issue, we model each snapshot as an individual slice, and concatenate all snapshots in a temporal dimension. As such, the received signals at the sparse URA  $\mathbb{P}_i$  can be represented as a three-dimensional (3-D) tensor

$$\mathcal{X}_i = \sum_{k=1}^K \mathbf{a}_i(\mu_k) \circ \mathbf{a}_i(\nu_k) \circ \mathbf{s}_k + \mathcal{N}_i \in \mathbb{C}^{M_{\mathbb{P}_i} \times N_{\mathbb{P}_i} \times T}, \quad (1)$$

where  $T$  denotes the number of snapshots,

$$\mathbf{a}_i(\mu_k) = [1, e^{-j\frac{2\pi}{\lambda}d_{x_i}\mu_k}, \dots, e^{-j\frac{2\pi}{\lambda}(M_{\mathbb{P}_i}-1)d_{x_i}\mu_k}]^T \in \mathbb{C}^{M_{\mathbb{P}_i}},$$

$$\mathbf{a}_i(\nu_k) = [1, e^{-j\frac{2\pi}{\lambda}d_{y_i}\nu_k}, \dots, e^{-j\frac{2\pi}{\lambda}(N_{\mathbb{P}_i}-1)d_{y_i}\nu_k}]^T \in \mathbb{C}^{N_{\mathbb{P}_i}} \quad (2)$$

are respectively the steering vectors along the  $x$ -axis and the  $y$ -axis with  $\mu_k = \sin \phi_k \cos \theta_k$ ,  $\nu_k = \sin \phi_k \sin \theta_k$ ,  $\mathbf{s}_k = [s_k(1), s_k(2), \dots, s_k(T)]^T \in \mathbb{C}^T$  is the signal waveform vector of the  $k$ -th source, and  $\mathcal{N}_i$  is an independent and identically distributed (i.i.d.) additive Gaussian white noise tensor, i.e.,  $\mathcal{N}_{i(\cdot, \cdot, t)} \sim \mathcal{CN}(\mathbf{0}, \sigma_n^2 \mathcal{I})$ ,  $\forall t \in \{1, 2, \dots, T\}$ . Here,  $\mathcal{N}_{i(\cdot, \cdot, t)}$  denotes the  $t$ -th slice of  $\mathcal{N}_i$ , and  $\sigma_n^2$  denotes the noise power. Note that, the signal component in (1) follows the canonical polyadic decomposition (CPD) representation.

To obtain the second-order signal statistics of the coprime planar array, we calculate a four-dimensional (4-D) cross-correlation tensor  $\mathcal{R} \in \mathbb{C}^{M_{\mathbb{P}_1} \times N_{\mathbb{P}_1} \times M_{\mathbb{P}_2} \times N_{\mathbb{P}_2}}$

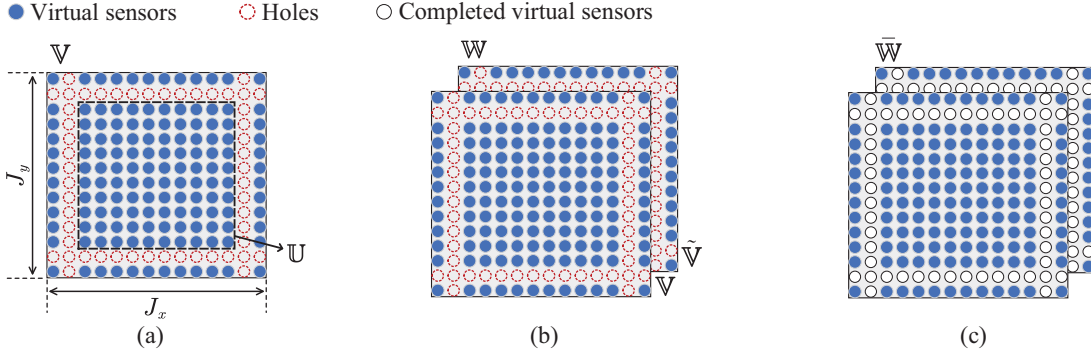


Fig. 2. The virtual array geometries of the coprime planar array. (a) The augmented virtual planar array  $\mathbb{V}$  and its continuous segment  $\mathbb{U}$ . (b) The discontinuous virtual cubic array  $\mathbb{W}$ . (c) The filled virtual cubic array  $\tilde{\mathbb{W}}$ .

between  $\mathcal{X}_1$  and  $\mathcal{X}_2$  as

$$\begin{aligned} \mathcal{R} &= \mathbb{E}\{\mathcal{X}_{1(\cdot,\cdot,\cdot,t)} \circ \mathcal{X}_{2(\cdot,\cdot,\cdot,t)}^*\} \\ &= \sum_{k=1}^K \sigma_{s_k}^2 \mathbf{a}_1(\mu_k) \circ \mathbf{a}_1(\nu_k) \circ \mathbf{a}_2^*(\mu_k) \circ \mathbf{a}_2^*(\nu_k) + \mathcal{N}, \end{aligned} \quad (3)$$

where  $\sigma_{s_k}^2 = \mathbb{E}\{s_k(t)s_k^*(t)\}$  represents the power of the  $k$ -th source, and  $\mathcal{N} = \mathbb{E}\{\mathcal{N}_{1(\cdot,\cdot,\cdot,t)} \circ \mathcal{N}_{2(\cdot,\cdot,\cdot,t)}^*\}$  is a 4-D zero tensor except the  $(1, 1, 1, 1)$ -th element being  $\sigma_n^2$ . In practices, the cross-correlation tensor  $\mathcal{R}$  can be estimated as

$$\hat{\mathcal{R}} = \frac{1}{T} \mathcal{X}_1 \underset{3}{\times} \mathcal{X}_2^*, \quad (4)$$

which averages the tensor contraction between  $\mathcal{X}_1$  and  $\mathcal{X}_2$  along the temporal dimension.

### III. Coarray Tensor Reformulation

In this section, we derive an incomplete coarray tensor from the cross-correlation tensor of the coprime planar array. To ensure an effective low-rank regularization on the slice-missing coarray tensor, we reformulate it as a structured one through shift dimensional augmenting and coarray tensor reshaping. Meanwhile, we also investigate the optimal shape of the reformulated coarray tensor.

#### A. Slice-missing coarray tensor derivation

In order to derive an augmented virtual array for DOA estimation, we merge the dimensions of the cross-correlation tensor  $\mathcal{R}$  that represent the angular information along the same coordinate axes to generate difference coarrays. More specifically, considering that the dimension pairs  $\{1, 3\}$  and  $\{2, 4\}$  of  $\mathcal{R}$  respectively represent the angular information along the  $x$ -axis and the  $y$ -axis,  $\mathcal{R}$  can be partially unfolded into a cross-correlation matrix  $\mathbf{R} \triangleq \mathcal{R}_{\{1,3\}\{2,4\}} \in \mathbb{C}^{M_{P_1} M_{P_2} \times N_{P_1} N_{P_2}}$  as

$$\mathbf{R} = \sum_{k=1}^K \sigma_{s_k}^2 [\mathbf{a}_2^*(\mu_k) \otimes \mathbf{a}_1(\mu_k)] \circ [\mathbf{a}_2^*(\nu_k) \otimes \mathbf{a}_1(\nu_k)] + \mathbf{Z}, \quad (5)$$

where Kronecker products  $\mathbf{a}_2^*(\mu_k) \otimes \mathbf{a}_1(\mu_k)$  and  $\mathbf{a}_2^*(\nu_k) \otimes \mathbf{a}_1(\nu_k)$  respectively derive difference coarrays along the

$x$ -axis and the  $y$ -axis, and  $\mathbf{Z} \triangleq \mathcal{N}_{\{1,3\}\{2,4\}}$  is a noise matrix with the  $(1, 1)$ -th element being  $\sigma_n^2$  while all others being 0.

As shown in Fig. 2(a), the difference coarrays generated in (5) correspond to an augmented discontinuous virtual planar array

$$\mathbb{V} = \{(x_{\mathbb{V}}, y_{\mathbb{V}}) | x_{\mathbb{V}} = d_{x_1} m_1 - d_{x_2} m_2, y_{\mathbb{V}} = d_{y_1} n_1 - d_{y_2} n_2\} \quad (6)$$

of size  $J_x \times J_y$ , where

$$\begin{aligned} J_x &= 3M_1 M_2 - M_1 - M_2 + 1, \\ J_y &= 3N_1 N_2 - N_1 - N_2 + 1. \end{aligned} \quad (7)$$

As such, the partially unfolding of  $\mathcal{R}$  in (5) enables the subsequent coarray tensor formulation. Denoting  $\mathbf{b}(\mu_k) \in \mathbb{C}^{J_x}$  and  $\mathbf{b}(\nu_k) \in \mathbb{C}^{J_y}$  respectively as the steering vectors of  $\mathbb{V}$  along the  $x$ -axis and the  $y$ -axis, they can be represented as

$$\mathbf{b}(\mu_k) = [e^{-j\pi(-M_1 M_2 + M_1)\mu_k}, e^{-j\pi(-M_1 M_2 + M_1 + 1)\mu_k}, \dots, e^{-j\pi(2M_1 M_2 - M_2)\mu_k}]^T \otimes \mathbf{e}_x, \quad (8)$$

and

$$\mathbf{b}(\nu_k) = [e^{-j\pi(-N_1 N_2 + N_1)\nu_k}, e^{-j\pi(-N_1 N_2 + N_1 + 1)\nu_k}, \dots, e^{-j\pi(2N_1 N_2 - N_2)\nu_k}]^T \otimes \mathbf{e}_y. \quad (9)$$

Here,  $\mathbf{e}_x$  is an all-one vector except the  $j_x$ -th element being 0 if  $j_x$  corresponds to the position of holes in  $\mathbb{V}$  along the  $x$ -axis, and  $\mathbf{e}_y$  is an all-one vector except the  $j_y$ -th element being 0 if  $j_y$  corresponds to the position of holes in  $\mathbb{V}$  along the  $y$ -axis. As shown in Fig. 2(a), the virtual planar array  $\mathbb{V}$  contains a virtual URA

$$\begin{aligned} \mathbb{U} &= \{(x_{\mathbb{U}}, y_{\mathbb{U}}) | x_{\mathbb{U}} = [-M_2 + 1, M_1 M_2 + M_1 - 1]d, \\ & \quad y_{\mathbb{U}} = [-N_2 + 1, N_1 N_2 + N_1 - 1]d\}, \end{aligned} \quad (10)$$

which was usually extracted for the Nyquist-matched coarray processing. This, however, causes an inevitable loss on statistical information. To avoid the information loss, we will make full use of all available virtual sensors in  $\mathbb{V}$  to achieve coarray tensor DOA estimation.

Since the cross-correlation statistics do not have the Hermitian property, the derived virtual planar array  $\mathbb{V}$  is geometrically non-symmetric to the coordinate axes. To

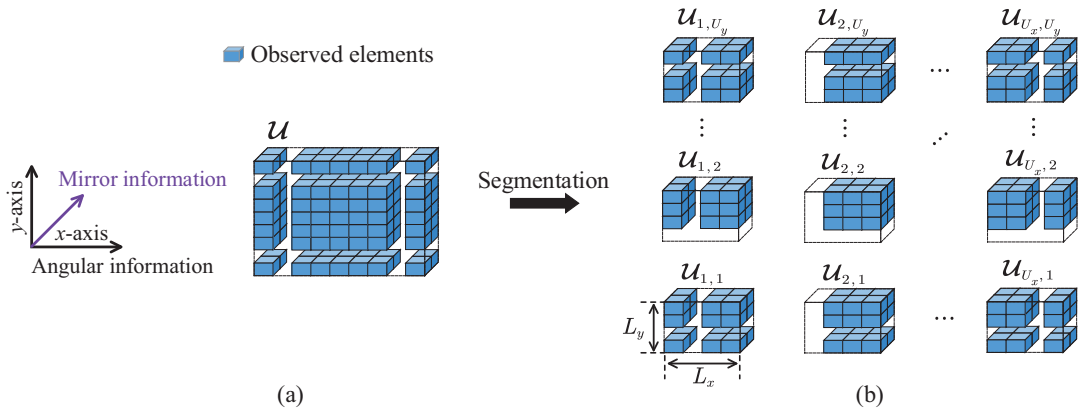


Fig. 3. Illustration of the proposed incomplete coarray tensor segmentation procedure. (a) The 3-D slice-missing coarray tensor  $\mathbf{U}$ . (b) The segmented coarray sub-tensors  $\mathbf{U}_{u_x, u_y}$ .

maximize the attainable virtual array aperture, we extend the mirror part of  $\mathbb{V}$  on the XOY plane, i.e.,  $\tilde{\mathbb{V}}$ , then pile up  $\mathbb{V}$  and  $\tilde{\mathbb{V}}$  to form a discontinuous virtual cubic array  $\mathbb{W}$ , as shown in Fig. 2(b). By sorting elements in the cross-correlation matrix  $\mathbf{R}$  to match the locations of virtual sensors in the virtual planar array  $\mathbb{V}$ , the equivalent second-order signal of  $\mathbb{V}$  can be obtained as  $\mathbf{U} \in \mathbb{C}^{J_x \times J_y}$ . Analogously, the equivalent second-order signal of the mirror virtual planar array  $\tilde{\mathbb{V}}$ , denoted by  $\tilde{\mathbf{U}} \in \mathbb{C}^{J_x \times J_y}$ , can be obtained by sorting elements in  $\mathbf{R}^*$ . Notably, the range of DOA estimation is determined by the deployment of the physical sensor array, and will not be affected by the virtual array configuration. Meanwhile, the derived virtual planar array  $\mathbb{V}$  and its mirror part  $\tilde{\mathbb{V}}$  are simultaneously utilized to expand the virtual array aperture, which does not influence the distinguishable range of DOA estimation.

Then, we concatenate  $\mathbf{U}$  and  $\tilde{\mathbf{U}}$  along the third dimension to derive the equivalent second order signal of the virtual cubic array  $\mathbb{W}$ , i.e., a 3-D incomplete coarray tensor

$$\mathbf{U} = \sum_{k=1}^K \sigma_{s_k}^2 \mathbf{b}(\mu_k) \circ \mathbf{b}(\nu_k) \circ \mathbf{h}_k + \mathbf{Z} \in \mathbb{C}^{J_x \times J_y \times 2}. \quad (11)$$

Here,

$$\mathbf{h}_k = [1, e^{-j\pi(-(M_1 M_2 + M_1 + M_2)\mu_k - (N_1 N_2 + N_1 + N_2)\nu_k)}]^T \quad (12)$$

is a mirror factor vector reflecting the relationship between  $\mathbb{V}$  and  $\tilde{\mathbb{V}}$ , and  $\mathbf{Z}$  is a noise tensor with the  $(M_2, N_2, 1)$ -th and the  $(M_1 M_2 + M_1, N_1 N_2 + N_1, 2)$ -th elements being  $\sigma_n^2$  while all others being 0.

It is observed from Fig. 2(a) that there exist holes in several rows and columns of  $\mathbb{V}$ , resulting in whole rows and columns of missing elements in  $\mathbf{U}$  and  $\tilde{\mathbf{U}}$ . Since the conventional matrix completion approaches require missing elements in an incomplete matrix to be randomly distributed, we cannot directly implement the matrix completion on  $\mathbf{U}$  or  $\tilde{\mathbf{U}}$ . Accordingly, there are lateral and horizontal slices of holes in  $\mathbb{W}$  as shown in Fig. 2(b), and the corresponding incomplete coarray

tensor  $\mathbf{U}$  possesses whole slices of missing elements, as illustrated in Fig. 3(a).

## B. Structured coarray tensor formulation

To exploit the enlarged virtual array aperture brought by the discontinuous virtual cubic array  $\mathbb{W}$ , the corresponding slice-missing coarray tensor  $\mathbf{U}$  should be completed, such that the coarray tensor processing can be implemented at the Nyquist rate. However, the existing low-rank tensor completion techniques under the premise of random missing pattern [30, 31] are not applicable here. In this regard, we propose shift dimensional augmenting and coarray tensor reshaping approaches to reformulate the coarray tensor  $\mathbf{U}$  as a structured one with dispersed missing elements.

To begin with, in order to distribute the slices of missing elements in  $\mathbf{U}$ , as shown in Fig. 3, we first segment  $\mathbf{U}$  into  $U_x \times U_y$  coarray sub-tensors  $\mathbf{U}_{u_x, u_y} \in \mathbb{C}^{L_x \times L_y \times 2}$  with the positions of extracted elements indexed by  $[u_x, u_x + L_x - 1]$ ,  $[u_y, u_y + L_y - 1]$ , and  $\{1, 2\}$  in three respective dimensions. Here, we have  $u_x \in \{1, 2, \dots, U_x\}$ ,  $u_y \in \{1, 2, \dots, U_y\}$ , and

$$U_x = J_x + 1 - L_x, \quad U_y = J_y + 1 - L_y. \quad (13)$$

Since the number of coarray sub-tensors  $U_x \geq 2$  and  $U_y \geq 2$ , the size of coarray sub-tensors satisfies

$$2 \leq L_x \leq J_x - 1, \quad 2 \leq L_y \leq J_y - 1. \quad (14)$$

By introducing two segmentation matrices

$$\mathbf{S}_{u_x} = \begin{bmatrix} \mathbf{0}_{(u_x-1) \times L_x} \\ \mathbf{I}_{L_x \times L_x} \\ \mathbf{0}_{(J_x-L_x-u_x+1) \times L_x} \end{bmatrix} \in \mathbb{C}^{J_x \times L_x}, \quad (15)$$

$$\mathbf{S}_{u_y} = \begin{bmatrix} \mathbf{0}_{(u_y-1) \times L_y} \\ \mathbf{I}_{L_y \times L_y} \\ \mathbf{0}_{(J_y-L_y-u_y+1) \times L_y} \end{bmatrix} \in \mathbb{C}^{J_y \times L_y}, \quad (16)$$

the coarray sub-tensor  $\mathbf{U}_{u_x, u_y}$  can be expressed as

$$\mathbf{U}_{u_x, u_y} = \mathbf{U} \times_1 \mathbf{S}_{u_x} \times_2 \mathbf{S}_{u_y}. \quad (17)$$

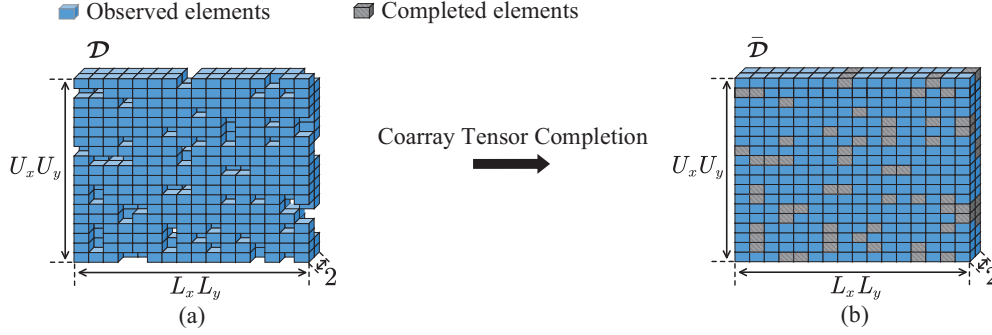


Fig. 4. Illustration of coarray tensor completion. (a) The reformulated coarray tensor  $\mathcal{D}$  with dispersed missing elements. (b) The completed coarray tensor  $\bar{\mathcal{D}}$ .

As depicted in Fig. 3(b), the coarray sub-tensors  $\mathbf{U}_{u_x, u_y}$  and  $\mathbf{U}_{u_x+1, u_y}$  have the same angular information along the  $y$ -axis, but a one-step shifting relationship along the  $x$ -axis. Thus,  $U_x$  coarray sub-tensors  $\mathbf{U}_{:, u_y}$  can be concatenated along the fourth dimension to generate a 4-D tensor

$$\mathcal{Q}_{u_y} = [\mathbf{U}_{1, u_y}, \mathbf{U}_{2, u_y}, \dots, \mathbf{U}_{U_x, u_y}]_{\sqcup_4} \in \mathbb{C}^{L_x \times L_y \times 2 \times U_x}, \quad (18)$$

$\forall u_y = 1, 2, \dots, U_y$ . Similarly, there is a one-step shifting relationship along the  $y$ -axis between 4-D tensors  $\mathcal{Q}_{u_y}$  and  $\mathcal{Q}_{u_y+1}$ . Hence, the  $U_y$  4-D tensors are further concatenated along the fifth dimension to formulate a five-dimensional (5-D) coarray tensor

$$\mathcal{T} = [\mathcal{Q}_1, \mathcal{Q}_2, \dots, \mathcal{Q}_{U_y}]_{\sqcup_5} \in \mathbb{C}^{L_x \times L_y \times 2 \times U_x \times U_y}, \quad (19)$$

whose five dimensions characterize the angular information along the  $x, y$ -axes, the mirror information, and the shifting information along the  $x, y$ -axes, respectively. As such, the segmented coarray sub-tensors of the coarray tensor  $\mathbf{U}$  have been concatenated to generate two additional shifting dimensions, and the missing elements are distributed across the total five dimensions.

Since the five dimensions of  $\mathcal{T}$  can be categorized into angular, shifting, and mirror dimensions, they can be structurally merged to construct a 3-D incomplete structured coarray tensor

$$\mathcal{D} \triangleq \mathcal{T}_{\{1,2\}, \{4,5\}, \{3\}} \in \mathbb{C}^{L_x L_y \times U_x U_y \times 2}, \quad (20)$$

as depicted in Fig. 4(a). The reformulated coarray tensor  $\mathcal{D}$  possesses structurally dispersed missing elements, which is demonstrated in the following *Proposition*.

*Proposition:* There is no missing slice in the reformulated coarray tensor  $\mathcal{D}$ , whose dispersed missing elements can be structurally mapped from the missing slices of  $\mathbf{U}$ .

*Proof:* Based on the proposed shift dimensional augmenting and coarray tensor reshaping approaches, the elements in the reformulated coarray tensor  $\mathcal{D}$  can be mapped from the initial coarray tensor  $\mathbf{U}$  as

$$\begin{aligned} \mathcal{D}_{(j_1, j_2, j_3)} &= \mathcal{T}_{(\text{mod}(j_1, L_x), [j_1/L_x], j_3, \text{mod}(j_2, U_x), [j_2/U_x])} \\ &= \mathbf{U}_{(\text{mod}(j_1, L_x) + \text{mod}(j_2, U_x) - 1, [j_1/L_x] + [j_2/U_x] - 1, j_3)}, \end{aligned} \quad (21)$$

where  $\mathcal{D}_{(j_1, j_2, j_3)}$  denotes the  $(j_1, j_2, j_3)$ -th element in  $\mathcal{D}$ ,  $j_1 \in \{1, 2, \dots, L_x L_y\}$ ,  $j_2 \in \{1, 2, \dots, U_x U_y\}$ , and  $j_3 \in$

$\{1, 2\}$ . Therefore, the positions of both observed elements and missing elements in  $\mathcal{D}$  are determined as long as the size of coarray sub-tensors  $(L_x, L_y)$  is given.

We then prove that there is no missing slice in the reformulated coarray tensor  $\mathcal{D}$  by contradiction. Assume that the  $j_1$ -th slice of elements in  $\mathcal{D}$  is entirely missing, i.e., for an invariant index  $j_1$  and  $\forall j_2 \in \{1, 2, \dots, U_x U_y\}$ ,  $\forall j_3 \in \{1, 2\}$ ,  $\mathcal{D}_{(j_1, j_2, j_3)}$  denotes missing elements. Then, according to the mapping relationship established in (21), the corresponding elements in the initial coarray tensor  $\mathbf{U}$ , i.e.,  $\mathbf{U}_{(\text{mod}(j_1, L_x) + \text{mod}(j_2, U_x) - 1, [j_1/L_x] + [j_2/U_x] - 1, j_3)}$ , is missing. For the incomplete coarray tensor  $\mathbf{U}$ , at least one of the indices  $\text{mod}(j_1, L_x) + \text{mod}(j_2, U_x) - 1$ ,  $[j_1/L_x] + [j_2/U_x] - 1$ ,  $j_3$  should be a fixed value to indicate its whole missing slices. However, none of these indices can be practically fixed with an invariant  $j_1$  and  $\forall j_2 \in \{1, 2, \dots, U_x U_y\}$ ,  $\forall j_3 \in \{1, 2\}$ , implying that the missing elements in  $\mathbf{U}$  are not concentrated in a single slice. This is in conflict with the fact that there are missing slices in  $\mathbf{U}$ . Thus, based on the contradiction analysis, the missing slice have been sufficiently dispersed in the reformulated coarray tensor  $\mathcal{D}$ . ■

### C. Coarray sub-tensor size selection

Although the size of the coarray sub-tensors  $\mathbf{U}_{u_x, u_y}$  can be selected within  $L_x \in [2, J_x - 1]$  and  $L_y \in [2, J_y - 1]$ , different  $(L_x, L_y)$  pairs will cause different positions of the dispersed missing elements, as well as their percentage in the reformulated coarray tensor  $\mathcal{D}$ . To complete  $\mathcal{D}$  in an effective manner, its dispersion level of missing elements should be as high as possible, while the percentage of missing elements should be as small as possible simultaneously.

Let  $\Omega$  be the index set of missing elements in  $\mathcal{D}$ , the dispersion level of missing elements can be measured by the summation of Euclidean distances between each pair of missing elements in  $\mathcal{D}$ , i.e.,

$$\psi = \sum_{\omega_1, \omega_2 \in \Omega, \omega_1 \neq \omega_2} \|\omega_1 - \omega_2\|_2, \quad (22)$$

where  $\omega_1, \omega_2$  denote the indices of a missing element pair. Meanwhile, the percentage of missing elements in  $\mathcal{D}$  can

be calculated as

$$\gamma = \frac{|\Omega|}{2L_x L_y U_x U_y}. \quad (23)$$

To satisfy the requirement for the utmost dispersion level and the least percentage of missing elements in  $\mathcal{D}$ , the size of coarray sub-tensors can be optimized by solving the following integer programming problem

$$\begin{aligned} \max_{L_x, L_y} \quad & \psi/\gamma \\ \text{s.t.} \quad & 2 \leq L_x \leq J_x - 1, \\ & 2 \leq L_y \leq J_y - 1, \quad L_x, L_y \in \mathbb{N}, \end{aligned} \quad (24)$$

where the objective function is the dispersion-to-percentage ratio (DPR) of missing elements in  $\mathcal{D}$ . The optimization problem can be efficiently solved by traversing  $L_x$  and  $L_y$  in their respective ranges  $[2, J_x - 1]$  and  $[2, J_y - 1]$  to find the maximum DPR of missing elements.

It is worth to point out that the optimal pair  $(L_x, L_y)$  remains fixed for a given coprime planar array geometry. Therefore, the optimal size of coarray sub-tensors  $\mathcal{U}_{u_x, u_y}$  can be determined off-line, and will not increase the computational complexity of DOA estimation.

#### IV. Coarray Tensor Completion for DOA Estimation

In this section, we elaborate a coarray tensor completion algorithm for 2-D DOA estimation. In particular, we impose a low-rank regularization on the reformulated coarray tensor to complete its missing elements. Then, we decompose the completed coarray tensor to estimate azimuth and elevation in closed-form solutions. Finally, we analyze the computational complexity of the proposed algorithm.

##### A. Coarray tensor completion

The low-rank regularization can now be imposed on the reformulated coarray tensor  $\mathcal{D}$  with an optimal shape. Based on the principle of tensor rank relaxation [35], low-rank coarray tensor completion can be formulated as a coarray tensor nuclear norm minimization problem

$$\begin{aligned} \min_{\bar{\mathcal{D}}} \quad & \|\bar{\mathcal{D}}\|_* = \sum_{j=1}^{o(\bar{\mathcal{D}})} \alpha_j \|\bar{\mathcal{D}}_{(j)}\|_* \\ \text{s.t.} \quad & P_{\bar{\Omega}}(\bar{\mathcal{D}}) = P_{\bar{\Omega}}(\mathcal{D}), \end{aligned} \quad (25)$$

where the optimization variable  $\bar{\mathcal{D}} \in \mathbb{C}^{L_x L_y \times U_x U_y \times 2}$  is the completed coarray tensor,  $\bar{\Omega}$  is the complement set of  $\Omega$ , i.e., the index set of observed elements in  $\mathcal{D}$ , and  $\alpha_j \geq 0$  is the non-negative weight satisfying  $\sum_{j=1}^{o(\bar{\mathcal{D}})} \alpha_j = 1$ . The optimization problem (25) aims to minimize the tensor nuclear norm of  $\bar{\mathcal{D}}$  under the constraint that all observed elements in  $\mathcal{D}$  are kept in  $\bar{\mathcal{D}}$ , where the coarray tensor nuclear norm is a convex combination of its matrix unfoldings' nuclear norms.

The convex optimization problem (25) cannot be directly solved because of the non-smooth and non-differentiable nuclear norm terms  $\|\bar{\mathcal{D}}_{(j)}\|_*$ . Hence, we

prefer to use ADMM, which can effectively solve large-scale optimization problems with multiple non-smooth terms in the objective [36]. In particular, to ensure that the three nuclear norm terms  $\|\bar{\mathcal{D}}_{(1)}\|_*$ ,  $\|\bar{\mathcal{D}}_{(2)}\|_*$  and  $\|\bar{\mathcal{D}}_{(3)}\|_*$  in the objective of (25) can be independently optimized, we introduce three auxiliary tensors  $\mathcal{Y}_1 = \mathcal{Y}_2 = \mathcal{Y}_3$  to transform the coarray tensor nuclear norm minimization problem (25) into an equivalent form

$$\begin{aligned} \min_{\bar{\mathcal{D}}, \mathcal{Y}_j} \quad & \|\bar{\mathcal{D}}\|_* \\ \text{s.t.} \quad & P_{\bar{\Omega}}(\bar{\mathcal{D}}) = P_{\bar{\Omega}}(\mathcal{D}), \\ & \mathcal{Y}_j - \bar{\mathcal{D}} = \mathcal{O}, \quad j \in \{1, 2, \dots, o(\bar{\mathcal{D}})\}. \end{aligned} \quad (26)$$

The detailed procedure of ADMM for solving the completed coarray tensor  $\bar{\mathcal{D}}$  in (26) can be found in Appendix A. The completed coarray tensor  $\bar{\mathcal{D}}$  shown in Fig. 4(b) corresponds to a filled virtual cubic array

$$\begin{aligned} \bar{\mathbb{W}} = \{ & (x_{\bar{\mathbb{W}}}, y_{\bar{\mathbb{W}}}, z_{\bar{\mathbb{W}}}) | x_{\bar{\mathbb{W}}} = [-M_1 M_2 + M_1, 2M_1 M_2 - M_2]d, \\ & y_{\bar{\mathbb{W}}} = [-N_1 N_2 + N_1, 2N_1 N_2 - N_2]d, \\ & z_{\bar{\mathbb{W}}} = [1, 2]d \}, \end{aligned} \quad (27)$$

as shown in Fig. 2(c).

The iterative ADMM procedure converges as long as the relative error of the completed coarray tensor between two successive iterations is less than a convergence threshold  $\xi_{\text{ADMM}} > 0$  [31], i.e.,

$$\frac{\|\bar{\mathcal{D}}^{(n_A+1)} - \bar{\mathcal{D}}^{(n_A)}\|_F}{\|\bar{\mathcal{D}}^{(n_A)}\|_F} \leq \xi_{\text{ADMM}}. \quad (28)$$

Here,  $\bar{\mathcal{D}}^{(n_A)}$  denotes the completed coarray tensor at the  $n_A$ -th iteration. The convergence of the proposed ADMM solution to coarray tensor completion satisfies the following theorem.

*Theorem 1:* The iterative completed coarray tensor sequence  $(\bar{\mathcal{D}}^{(n_A)}, \mathcal{Y}_j^{(n_A)})$  generated by the ADMM for coarray tensor completion is convergent.

*Proof:* By introducing the indicator function

$$\mathbf{1}_{\bar{\Omega}}(\bar{\mathcal{D}}_{(j_1, j_2, j_3)}) = \begin{cases} 0, & \text{if } (j_1, j_2, j_3) \in \bar{\Omega}, \\ 1, & \text{if } (j_1, j_2, j_3) \notin \bar{\Omega}, \end{cases} \quad (29)$$

to substitute the constraint  $P_{\bar{\Omega}}(\bar{\mathcal{D}}) = P_{\bar{\Omega}}(\mathcal{D})$ , (26) can be equivalently represented as

$$\begin{aligned} \min_{\bar{\mathcal{D}}, \mathcal{Y}_j} \quad & \|\bar{\mathcal{D}}\|_* + \mathbf{1}_{\bar{\Omega}}(\bar{\mathcal{D}}) \\ \text{s.t.} \quad & \mathcal{Y}_j \times_1 \mathbf{I}_{J_x \times J_x}^{(1)} \times_2 \mathbf{I}_{J_y \times J_y}^{(1)} \times_3 \mathbf{I}_{2 \times 2}^{(1)} \\ & - \bar{\mathcal{D}} \times_1 \mathbf{I}_{J_x \times J_x}^{(2)} \times_2 \mathbf{I}_{J_y \times J_y}^{(2)} \times_3 \mathbf{I}_{2 \times 2}^{(2)} = \mathcal{O}. \end{aligned} \quad (30)$$

By multiplying  $\mathcal{Y}_j$  and  $\bar{\mathcal{D}}$  with identity matrices  $\mathbf{I}^{(1)}$  and  $\mathbf{I}^{(2)}$ , the constraint in (30) equals to the constraint  $\mathcal{Y}_j - \bar{\mathcal{D}} = \mathcal{O}$  in (26). We then demonstrate that the reformulated optimization problem (30) satisfies the following properties, which are the necessary conditions for the global convergence of ADMM [37].

**A1. Coercivity:** For the feasible set

$$\Theta = \{(\bar{\mathcal{D}}, \mathcal{Y}_j) : \mathcal{Y}_j - \bar{\mathcal{D}} = \mathcal{O}\}, \quad (31)$$

$$\|\bar{\mathcal{D}}\|_* + \mathbf{1}_{\bar{\Omega}}(\bar{\mathcal{D}}) \text{ is coercive over } \Theta, \text{ i.e.,} \\ \|\bar{\mathcal{D}}\|_* + \mathbf{1}_{\bar{\Omega}}(\bar{\mathcal{D}}) \rightarrow \infty, \quad (32)$$

if  $(\bar{\mathcal{D}}, \mathcal{Y}_j) \in \Theta$  and  $\|(\bar{\mathcal{D}}, \mathcal{Y}_j)\|_2 \rightarrow \infty$ . Here, the notation  $\rightarrow \infty$  represents tending to infinity.

**A2. Feasibility:** Since the coefficient matrices of  $\mathcal{Y}_j$  and  $\bar{\mathcal{D}}$  are both identity matrices, we have  $\mathbf{I}^{(1)} \subseteq \mathbf{I}^{(2)}$ . Hence, the feasibility of (30) holds.

**A3. Lipschitz sub-minimization paths:** For any fixed  $\bar{\mathcal{D}}, \mathcal{E}_1 : \mathbf{I}^{(1)} \rightarrow \mathbb{C}^{J_x \times J_y \times 2}$  obeying

$$\mathcal{E}_1(\mathcal{G}) = \underset{\mathcal{Y}_j}{\operatorname{argmin}} \left\{ \|\mathcal{Y}_j\|_* + \mathbf{1}_{\bar{\Omega}}(\bar{\mathcal{D}}) : \right. \\ \left. \mathcal{Y}_j \times_1 \mathbf{I}_{J_x \times J_x}^{(1)} \times_2 \mathbf{I}_{J_y \times J_y}^{(1)} \times_3 \mathbf{I}_{2 \times 2}^{(1)} = \mathcal{G} \right\} \quad (33)$$

is a Lipschitz continuous map. Similarly, for any fixed  $\mathcal{Y}_j, \mathcal{E}_2 : \mathbf{I}^{(2)} \rightarrow \mathbb{C}^{J_x \times J_y \times 2}$  obeying

$$\mathcal{E}_2(\mathcal{G}) = \underset{\bar{\mathcal{D}}}{\operatorname{argmin}} \left\{ \|\mathcal{Y}_j\|_* + \mathbf{1}_{\bar{\Omega}}(\bar{\mathcal{D}}) : \right. \\ \left. \bar{\mathcal{D}} \times_1 \mathbf{I}_{J_x \times J_x}^{(2)} \times_2 \mathbf{I}_{J_y \times J_y}^{(2)} \times_3 \mathbf{I}_{2 \times 2}^{(2)} = \mathcal{G} \right\} \quad (34)$$

is a Lipschitz continuous map.

**A4. Objective- $\|\cdot\|_*$  regularity:** The coarray tensor nuclear norm function  $\|\bar{\mathcal{D}}\|_*$  is Lipschitz differentiable [38], such that the regularity of the objective  $\|\bar{\mathcal{D}}\|_*$  holds.

**A5. Objective- $\mathbf{1}_{\bar{\Omega}}(\cdot)$  regularity:** The indicator function  $\mathbf{1}_{\bar{\Omega}}(\bar{\mathcal{D}})$  is lower semi-continuous [37], such that the regularity of the objective  $\mathbf{1}_{\bar{\Omega}}(\bar{\mathcal{D}})$  holds.

Since the coarray tensor completion problem (30) fits the properties A1~A5, the iterative completed coarray tensor sequence  $(\bar{\mathcal{D}}^{(n_A)}, \mathcal{Y}_j^{(n_A)})$  generated by the ADMM solution for coarray tensor completion is convergent. ■

## B. DOA estimation via coarray tensor CPD

Since the completed coarray tensor  $\bar{\mathcal{D}}$  corresponds to the filled virtual cubic array  $\bar{\mathbb{W}}$  with uniformly spaced virtual sensors, the CPD can be applied to  $\bar{\mathcal{D}}$  to retrieve the elevation and azimuth of sources. In particular, to obtain a CPD representation of  $\bar{\mathcal{D}}$ , we first define the completed version of the initial coarray tensor  $\mathcal{U}$ , i.e.,  $\bar{\mathcal{U}}$ . According to the definition of  $\mathcal{U}$  in (11), its completed version  $\bar{\mathcal{U}}$  can be represented as

$$\bar{\mathcal{U}} = \sum_{k=1}^K \sigma_{s_k}^2 \bar{\mathbf{b}}(\mu_k) \circ \bar{\mathbf{b}}(\nu_k) \circ \mathbf{h}_k + \bar{\mathcal{Z}}, \quad (35)$$

where

$$\bar{\mathbf{b}}(\mu_k) = \left[ e^{-j\pi(-M_1M_2+M_1)\mu_k}, e^{-j\pi(-M_1M_2+M_1+1)\mu_k}, \right. \\ \left. \dots, e^{-j\pi(2M_1M_2-M_2)\mu_k} \right]^T \quad (36)$$

and

$$\bar{\mathbf{b}}(\nu_k) = \left[ e^{-j\pi(-N_1N_2+N_1)\nu_k}, e^{-j\pi(-N_1N_2+N_1+1)\nu_k}, \right. \\ \left. \dots, e^{-j\pi(2N_1N_2-N_2)\nu_k} \right]^T \quad (37)$$

are respectively the steering vectors of the filled virtual cubic array  $\bar{\mathbb{W}}$  along the  $x$ -axis and the  $y$ -axis, and  $\bar{\mathcal{Z}}$  is a residual noise tensor after the coarray tensor completion.

Then, similar to the shift dimensional augmenting from 3-D coarray tensor  $\mathcal{U}$  to 5-D augmented coarray tensor  $\mathcal{T}$  in Section III.B, the completed version of  $\mathcal{T}$  can be constructed from  $\bar{\mathcal{U}}$  as

$$\bar{\mathcal{T}} = \sum_{k=1}^K \sigma_{s_k}^2 \mathbf{v}(\mu_k) \circ \mathbf{v}(\nu_k) \circ \mathbf{h}_k \circ \mathbf{g}(\mu_k) \circ \mathbf{g}(\nu_k) + \bar{\mathcal{B}}. \quad (38)$$

Here,

$$\mathbf{v}(\mu_k) = \left[ e^{-j\pi(-M_1M_2+M_1)\mu_k}, e^{-j\pi(-M_1M_2+M_1+1)\mu_k}, \right. \\ \left. \dots, e^{-j\pi(-M_1M_2+M_1+L_x-1)\mu_k} \right]^T \quad (39)$$

and

$$\mathbf{v}(\nu_k) = \left[ e^{-j\pi(-N_1N_2+N_1)\nu_k}, e^{-j\pi(-N_1N_2+N_1+1)\nu_k}, \right. \\ \left. \dots, e^{-j\pi(-N_1N_2+N_1+L_y-1)\nu_k} \right]^T \quad (40)$$

are respectively the steering vectors of the subarray

$$\bar{\mathbb{W}}_s = \{ (x_{\bar{\mathbb{W}}_s}, y_{\bar{\mathbb{W}}_s}, z_{\bar{\mathbb{W}}_s}) \} \\ x_{\bar{\mathbb{W}}_s} = [-M_1M_2+M_1, -M_1M_2+M_1+L_x-1]d, \\ y_{\bar{\mathbb{W}}_s} = [-N_1N_2+N_1, -N_1N_2+N_1+L_y-1]d, \\ z_{\bar{\mathbb{W}}_s} = [1, 2]d \} \quad (41)$$

segmented from  $\bar{\mathbb{W}}$  along the  $x$ -axis and the  $y$ -axis,

$$\mathbf{g}(\mu_k) = [1, e^{-j\pi\mu_k}, \dots, e^{-j\pi(U_x-1)\mu_k}]^T, \\ \mathbf{g}(\nu_k) = [1, e^{-j\pi\nu_k}, \dots, e^{-j\pi(U_y-1)\nu_k}]^T \quad (42)$$

are respectively the shifting vectors along the  $x$ -axis and the  $y$ -axis, and  $\bar{\mathcal{B}}$  is a 5-D residual noise tensor generated from the shift dimensional augmenting on  $\bar{\mathcal{Z}}$ . Following the coarray tensor reshaping procedure (20), the completed coarray tensor  $\bar{\mathcal{D}}$  can be obtained as

$$\bar{\mathcal{D}} \triangleq \bar{\mathcal{T}}_{\{1,2\},\{4,5\},\{3\}} = \sum_{k=1}^K \sigma_{s_k}^2 \mathbf{v}_k \circ \mathbf{g}_k \circ \mathbf{h}_k + \bar{\mathcal{B}}, \quad (43)$$

where

$$\mathbf{v}_k = \mathbf{v}(\nu_k) \otimes \mathbf{v}(\mu_k) \in \mathbb{C}^{L_x L_y}, \\ \mathbf{g}_k = \mathbf{g}(\nu_k) \otimes \mathbf{g}(\mu_k) \in \mathbb{C}^{U_x U_y}, \quad (44)$$

are respectively the CP factors characterizing the angular and shifting information, and  $\bar{\mathcal{B}} \triangleq \mathcal{B}_{\{1,2\},\{4,5\},\{3\}}$  is the corresponding reshaped 3-D residual noise tensor.

Hence, applying CPD to the completed coarray tensor  $\bar{\mathcal{D}}$  (43) yields the estimated CP factors  $\hat{\mathbf{v}}_k, \hat{\mathbf{g}}_k$  and  $\hat{\mathbf{h}}_k$ . The detail in the CPD-based estimation of these factors is provided in Appendix B. Then, by exploiting the Kronecker structure of  $\hat{\mathbf{v}}_k$  and  $\hat{\mathbf{g}}_k$  in (44),  $\hat{\mu}_k$  and  $\hat{\nu}_k$  can be estimated as

$$\hat{\mu}_k = \left[ \angle \left( \frac{\hat{\mathbf{v}}_k(\zeta_1+1)}{\hat{\mathbf{v}}_k(\zeta_1)} \right) + \angle \left( \frac{\hat{\mathbf{g}}_k(\zeta_2+1)}{\hat{\mathbf{g}}_k(\zeta_2)} \right) \right] / (2\pi), \\ \hat{\nu}_k = \left[ \angle \left( \frac{\hat{\mathbf{v}}_k(L_x+\iota_1)}{\hat{\mathbf{v}}_k(\iota_1)} \right) + \angle \left( \frac{\hat{\mathbf{g}}_k(U_x+\iota_2)}{\hat{\mathbf{g}}_k(\iota_2)} \right) \right] / (2\pi), \quad (45)$$

where  $\operatorname{mod}(\zeta_1, L_y) \neq 0, \exists \zeta_1 \in \{1, 2, \dots, L_x L_y - 1\}$ ,  $\operatorname{mod}(\zeta_2, U_y) \neq 0, \exists \zeta_2 \in \{1, 2, \dots, U_x U_y - 1\}$ , and  $\iota_1 \in \{1, 2, \dots, L_x L_y - L_x\}$ ,  $\iota_2 \in \{1, 2, \dots, U_x U_y - U_x\}$ . Here,  $\hat{\mathbf{v}}_{k(\zeta_1)}$  denotes the  $\zeta_1$ -th element in  $\hat{\mathbf{v}}_k$ . Note that, the

CPD of  $\tilde{\mathcal{D}}$  is unique only up to scaling and permutation ambiguities. The permutation ambiguity of the estimated CP factors amounts to shuffling the sequence of sources, which does not influence the DOA estimation. On the other hand, the scaling ambiguity of the estimated CP factors can be resolved by the scaling normalization during the retrieval of  $\hat{\mu}_k$  and  $\hat{\nu}_k$  in (45). Specifically, one row of the estimated CP factor are divided by its previous row to retrieve  $\hat{\mu}_k$  and  $\hat{\nu}_k$ , e.g.,  $\hat{\mathbf{v}}_{k(\zeta_1+1)}/\hat{\mathbf{v}}_{k(\zeta_1)}$ , which normalizes the scaling. As such, the estimated CP factors are immune to both scaling and permutation ambiguities. According to the relationship between  $(\theta_k, \phi_k)$  and  $(\mu_k, \nu_k)$  established in Section II, the closed-form solution to the azimuth and elevation of the  $k$ -th source is given by

$$\begin{aligned}\hat{\theta}_k &= \arctan(\hat{\nu}_k/\hat{\mu}_k), \\ \hat{\phi}_k &= \arcsin\left(\sqrt{\hat{\mu}_k^2 + \hat{\nu}_k^2}\right).\end{aligned}\quad (46)$$

### C. Computational complexity analysis

As discussed above, the proposed algorithm mainly involves cross-correlation tensor calculation, coarray tensor completion, and coarray tensor decomposition, whose computational complexities are  $\mathcal{O}(M_1M_2N_1N_2T)$ ,  $\mathcal{O}((L_xL_y+U_xU_y)L_xL_yU_xU_yN_{\text{ADMM}})$  and  $\mathcal{O}((K^3+L_xL_yU_xU_y)KN_{\text{CPD}})$ , respectively. Here,  $N_{\text{ADMM}}$  and  $N_{\text{CPD}}$  denote the number of iterations for the ADMM solution and the completed coarray tensor CPD, respectively. Since the computational complexities of the latter two have a higher order than that of the first one, the computational complexity of the proposed algorithm is given as  $\mathcal{O}((L_xL_y+U_xU_y)L_xL_yU_xU_yN_{\text{ADMM}}+L_xL_yU_xU_yKN_{\text{CPD}})$ .

In comparison with the matrix-based methods, the computational complexity of the 2-D MUSIC method [39] is  $\mathcal{O}(N_{\text{MG}}(M_1N_1(M_1N_1-K)+M_2N_2(M_2N_2-K)))$ , where  $N_{\text{MG}}$  is the total number of spectral peak searching grids. The computational complexity of the coarray sparsity method [40] is  $\mathcal{O}(K^3N_{\text{SR}}N_{\text{SG}}^3)$ , where  $N_{\text{SR}}$  and  $N_{\text{SG}}$  are respectively the numbers of iterations and spatial sampling grids. For 2-D DOA estimation, both the ADMM for coarray tensor completion and the CPD of the completed coarray tensor efficiently converge within hundreds of iterations, whereas the number of either spectral peak searching grids or sampling grids has an order of  $10^6$  with the interval of grids being  $0.1^\circ$ . Hence, we have both  $N_{\text{MG}}, N_{\text{SG}} \gg M_i, N_i$  and  $N_{\text{MG}}, N_{\text{SG}} \gg N_{\text{ADMM}}, N_{\text{CPD}}$ . This indicates that the computational complexity of the proposed algorithm is lower than those of the 2-D MUSIC and coarray sparsity methods. Therefore, although the coarray tensor model operates on the multi-dimensional signal statistics, the proposed algorithm is still more computationally efficient than the matrix-based methods.

In comparison with the coarray tensor MUSIC method [41], its computational complexity can be calculated as  $\mathcal{O}((K^3+J_xJ_y)KN_{\text{CPD}}+N_{\text{MG}}(M_1N_1(M_1N_1-K)+M_2N_2(M_2N_2-K)))$ . Similarly, since  $N_{\text{MG}} \gg M_i, N_i$  and

$N_{\text{MG}} \gg N_{\text{ADMM}}, N_{\text{CPD}}$ , the required exhausting spectrum searching procedure for the coarray tensor MUSIC method makes it more costly than the proposed algorithm with a closed-form solution.

In summary, although the proposed algorithm includes tensor modeling and tensorial optimization, a closed-form solution is available for the proposed algorithm via the completed coarray tensor decomposition to avoid either spectral peak searching or sampling gridding. As such, it has a moderate computational complexity compared to the conventional matrix-based and tensor-based methods.

### V. Simulation

In the simulations, we consider a coprime planar array with  $M_1 = 2$ ,  $N_1 = 3$ ,  $M_2 = 3$ , and  $N_2 = 4$ . Hence, the total number of sensors is 35. Accordingly, the size of the discontinuous virtual cubic array  $\mathbb{W}$  is  $14 \times 30 \times 2$ . The weights defining the coarray tensor nuclear norm are set to  $\alpha_1 = \alpha_2 = \alpha_3 = 1/3$  in the coarray tensor nuclear norm minimization problem (25). The penalty constant in the augmented Lagrangian function of ADMM is set to  $\rho = 10^{-4}$ , and the positive constant to iteratively increase  $\rho$  is fixed at  $u = 1.1$ . The convergence thresholds of the ADMM and the coarray tensor CPD are set to  $\xi_{\text{ADMM}} = 10^{-12}$  and  $\xi_{\text{CPD}} = 10^{-12}$ , respectively. Unless otherwise specified, we present simulation results in two scenarios, namely, the number of snapshots is fixed at  $T = 300$  when the signal-to-noise ratio (SNR) varies, and the SNR is fixed to 0 dB when the number of snapshots varies. For each scenario,  $N_{\text{MC}} = 1,000$  Monte Carlo trials are run. All evaluated methods are implemented with MATLAB<sup>1</sup>.

#### A. Performance of the proposed algorithm with the optimal coarray sub-tensor size

We first select the optimal coarray sub-tensor size according to the integer programming problem (24). Considering that  $J_x = 14$  and  $J_y = 30$ , there are total 336 different combinations for the possible size  $(L_x, L_y)$ , among which the pair of  $(L_x, L_y) = (7, 14)$  has the maximum DPR of missing elements while the pair of  $(L_x, L_y) = (13, 2)$  has the minimum DPR. For the reference, we list a few candidate pairs and their corresponding DPRs in TABLE II.

To verify the effectiveness of the proposed coarray sub-tensor size selection strategy, in Fig. 5, we compare the DOA estimation performance of the proposed coarray tensor completion algorithm using different size pairs listed in TABLE II. The root-mean-square error (RMSE)

$$\text{RMSE} = \sqrt{\frac{1}{2KN_{\text{MC}}} \sum_{n_{\text{MC}}=1}^{N_{\text{MC}}} \sum_{k=1}^K [(\hat{\theta}_{k, n_{\text{MC}}} - \theta_k)^2 + (\hat{\phi}_{k, n_{\text{MC}}} - \phi_k)^2]}, \quad (47)$$

<sup>1</sup>The MATLAB code of the proposed algorithm is available at <https://github.com/HangZheng98/Coarray-Tensor-Completion-for-DOA-Estimation>.

TABLE II  
THE DISPERSION-TO-PERCENTAGE RATIO CORRESPONDING TO DIFFERENT COARRAY SUB-TENSOR SIZE

$(L_x, L_y)$	(13, 2)	(2, 3)	(5, 28)	(13, 27)	(10, 4)	(4, 5)	(8, 8)	(7, 14)
DPR (dB)	76.03	86.49	87.48	88.17	89.92	92.56	94.56	95.91

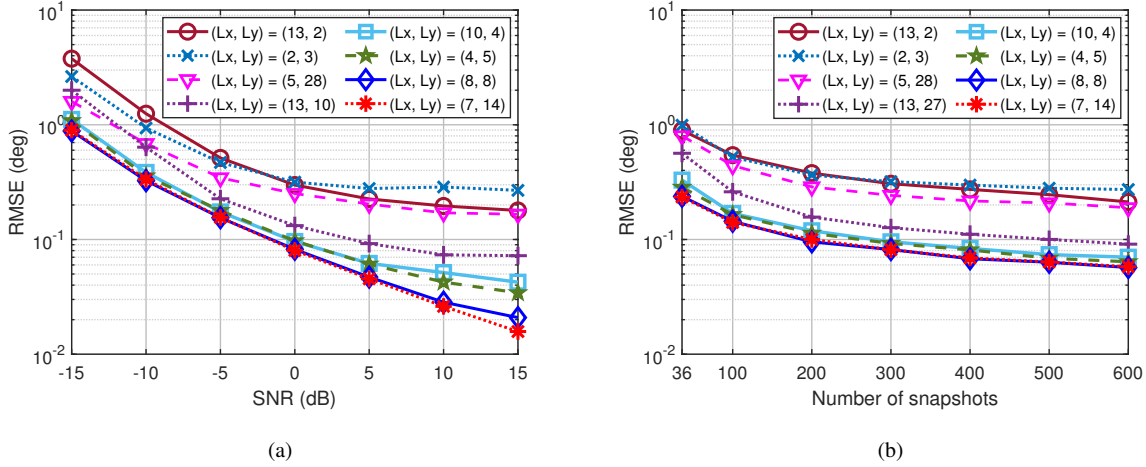


Fig. 5. DOA estimation performance of the proposed algorithm with different coarray sub-tensor sizes. (a) RMSE versus SNR. (b) RMSE versus the number of snapshots.

is adopted as the performance evaluation metric, where  $(\hat{\theta}_k, \hat{\phi}_k)$  is the estimate of  $(\theta_k, \phi_k)$  for the  $n_{MC}$ -th Monte Carlo trial. In this simulation,  $K = 2$  sources are assumed from the directions  $(\theta_1, \phi_1) = (25.6^\circ, 30.6^\circ)$  and  $(\theta_2, \phi_2) = (50.5^\circ, 40.5^\circ)$ , respectively.

It is observed from Fig. 5 that, as we predicted, the coarray sub-tensor size pair  $(L_x, L_y) = (7, 14)$  with the maximum DPR of missing elements depicts the best estimation accuracy. In contrast, the size pair  $(L_x, L_y) = (13, 2)$  with the minimum DPR has the worst estimation accuracy. Generally speaking, the higher the DPR, the better the DOA estimation accuracy. In the following simulations, the size of coarray sub-tensors  $\mathcal{U}_{u_x, u_y}$  will be fixed to  $7 \times 14 \times 2$ , leading the reformulated coarray tensor  $\mathcal{D} \in \mathbb{C}^{56 \times 238 \times 2}$ .

## B. Estimation accuracy comparison

Now we compare the DOA estimation performance of the proposed coarray tensor completion algorithm to the matrix-based methods including the 2-D MUSIC method [39], the coarray sparsity method ('Co-Sparsity') [40], the coarray ESPRIT method ('Co-ESPRIT') [17] and the coarray covariance matrix completion method ('Co-CMC') [28], as well as the tensor-based methods including the 2-D PARAFAC method [42] and the coarray tensor MUSIC method ('Co-T-MUSIC') [41]. Specifically, the 2-D MUSIC method adopts the idea of coprime subarray decomposition [43] for ambiguity-free DOA estimation without deriving coarray statistics. In contrast, both the

coarray sparsity and coarray ESPRIT methods derive vectorized coarray signals, then respectively implement sparse recovery optimization and ESPRIT on the coarray covariance matrix. However, they directly extract the continuous part of the augmented virtual array rather than interpolating it. In this regard, the coarray covariance matrix completion method applies low-rank matrix completion to the incomplete coarray covariance matrix to obtain an interpolated virtual array. As for the tensor-based methods, the 2-D PARAFAC method extends the idea of coprime subarray decomposition to the tensorial domain, while the coarray tensor MUSIC method only exploits the continuous coarray tensor statistics for enhanced DOA estimation. In addition, the Cramér-Rao bound for 2-D DOA estimation with the coprime planar array [44, 45] is also presented as the reference. The interval of the spectral peak searching grids for the 2-D MUSIC method and the coarray tensor MUSIC method, as well as the interval of the pre-defined sampling grids for the coarray sparsity method are set to  $0.1^\circ$ . The other simulation settings are the same as those in the first simulation. The RMSEs of azimuth angle estimation

$$\text{RMSE}_\theta = \sqrt{\frac{1}{KN_{MC}} \sum_{n_{MC}=1}^{N_{MC}} \sum_{k=1}^K (\hat{\theta}_{k, n_{MC}} - \theta_k)^2} \quad (48)$$

and elevation angle estimation

$$\text{RMSE}_\phi = \sqrt{\frac{1}{KN_{MC}} \sum_{n_{MC}=1}^{N_{MC}} \sum_{k=1}^K (\hat{\phi}_{k, n_{MC}} - \phi_k)^2} \quad (49)$$

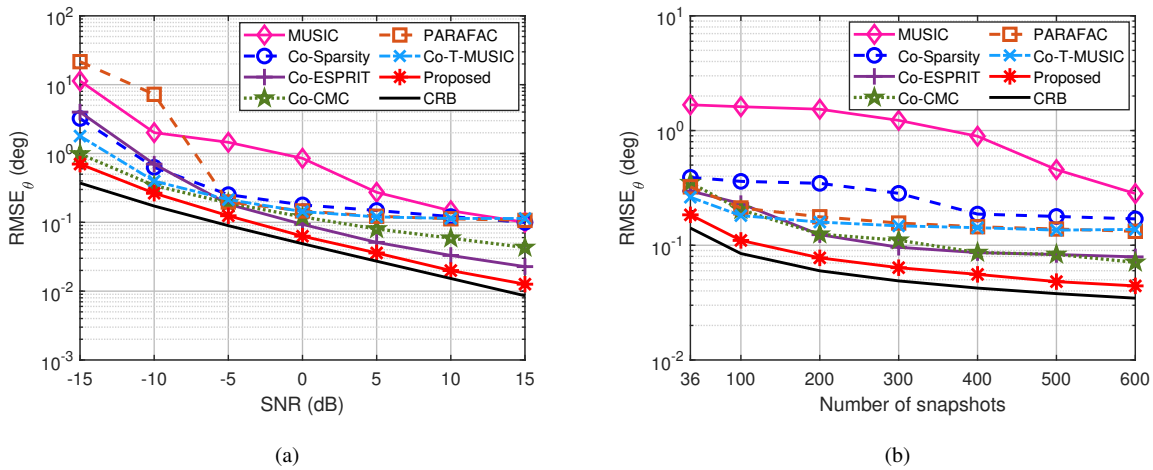


Fig. 6. Estimation accuracy comparison of the azimuth angle. (a)  $RMSE_{\theta}$  versus SNR. (b)  $RMSE_{\theta}$  versus the number of snapshots.

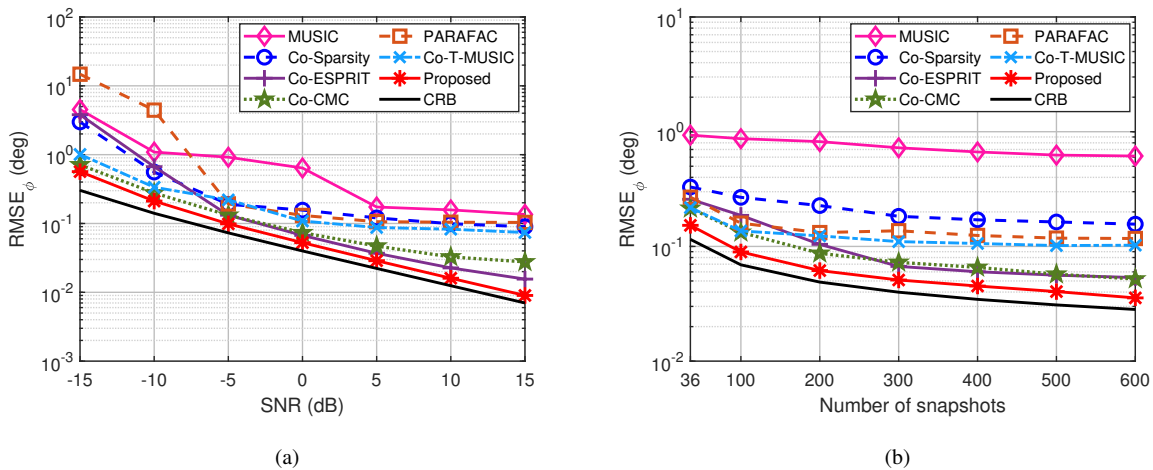


Fig. 7. Estimation accuracy comparison of the elevation angle. (a)  $RMSE_{\phi}$  versus SNR. (b)  $RMSE_{\phi}$  versus the number of snapshots.

are respectively compared in Fig. 6 and Fig. 7.

The coarray sparsity and coarray ESPRIT methods yield a remarkable improvement in estimation accuracy compared to the 2-D MUSIC method. Indeed, the coarray processing offers an augmented virtual array to improve the estimation accuracy, whereas the coprime subarray decomposition approach reduces the effective physical array aperture and sensor number for ambiguity elimination. Furthermore, by interpolating the discontinuous virtual array, the coarray covariance matrix completion method improves the estimation accuracy compared to the coarray sparsity method, and also outperforms the coarray ESPRIT method in most of the simulated scenarios including SNR range or snapshots. Likewise, the coarray tensor MUSIC method also presents an enhanced performance compared to both the 2-D MUSIC and 2-D PARAFAC methods by extending coarray processing to

the tensorial domain. Also, it is worth mentioning that the utilization of multi-dimensional tensor statistics benefits the 2-D DOA estimation, such that the 2-D PARAFAC method outperforms the 2-D MUSIC method, and the coarray tensor MUSIC method outperforms both the 2-D MUSIC and coarray sparsity methods. Limited by the fixed spectral peak searching grid, the coarray tensor MUSIC method is inferior to the coarray ESPRIT method when the SNR increases.

Compared to the competing matrix-based methods, the proposed coarray tensor completion algorithm presents the best accuracy over the simulated SNR range or snapshots. It is because the proposed algorithm effectively exploits structural signal characteristics of the coarray statistics, which is ignored by the matrix-based approaches. Similarly, the proposed algorithm achieves a significant improvement in estimation accuracy compared

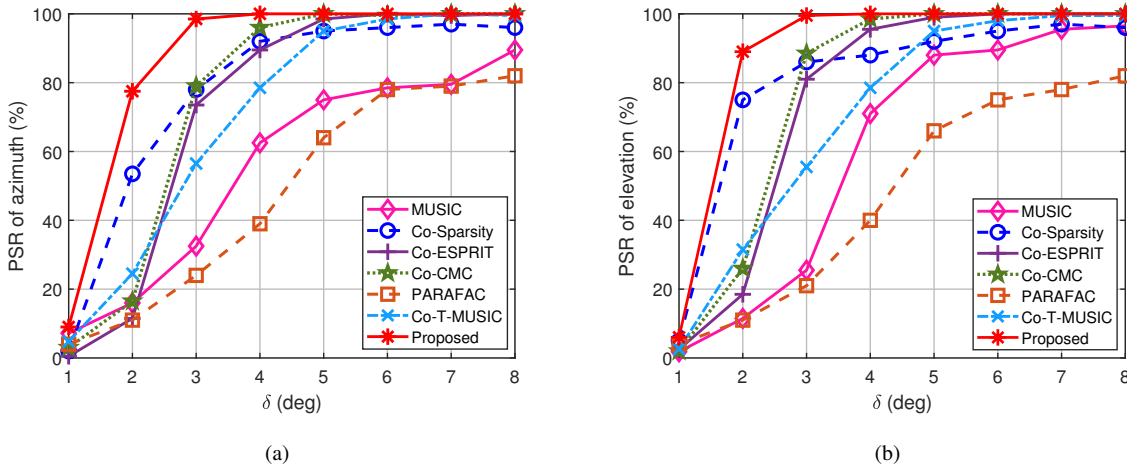


Fig. 8. Angular resolution comparison. (a) PSR of azimuth *versus* the angular spacing  $\delta$ . (b) PSR of elevation *versus* the angular spacing  $\delta$ .

to the competing tensor-based methods, which owes to the utilization of the entire discontinuous virtual cubic array  $\mathbb{W}$  via the coarray tensor completion. In contrast, the 2-D PARAFAC method does not exploit the coarray tensor statistics, while the coarray tensor MUSIC method only considers the continuous part of the derived virtual array.

### C. Angular resolution comparison

In Fig. 8, we compare the angular resolution of all evaluated methods by considering two closely separated sources  $(\theta_1, \phi_1)$  and  $(\theta_2, \phi_2)$  with an angular spacing of  $\delta$ . Specifically, both  $\theta_1$  and  $\phi_1$  are randomly selected between  $[20^\circ, 40^\circ]$  for each trial, while  $\theta_2$  and  $\phi_2$  respectively maintain angular spacings of  $\delta_\theta$  and  $\delta_\phi$  with  $\theta_1$  and  $\phi_1$ , i.e.,  $(\theta_2, \phi_2) = (\theta_1 + \delta_\theta, \phi_1 + \delta_\phi)$ . Here,  $\delta_\theta$  is randomly generated within  $[0, \delta]$ , while  $\delta_\phi$  is then calculated to satisfy  $\sqrt{\delta_\theta^2 + \delta_\phi^2} = \delta$ . Two sources are regarded as distinguishable respectively on the azimuth domain and on the elevation domain if  $|\hat{\theta}_{k,n_{MC}} - \theta_k| < \delta/2$  and  $|\hat{\phi}_{k,n_{MC}} - \phi_k| < \delta/2$  for each trial. The probabilities of successful resolution (PSRs) of azimuth and elevation can be respectively calculated as the percentages of successful trials.

It is clear that the coarray-based methods, namely, the coarray sparsity method, the coarray ESPRIT method and the coarray tensor MUSIC method, present higher angular resolutions compared to the coprime subarray decomposition-based methods, namely, the 2-D MUSIC method and the 2-D PARAFAC method. It is also noted that, the coarray covariance matrix completion method presents a further improvement in angular resolution compared to the coarray ESPRIT method. These phenomena owe to the enlarged virtual array aperture compared to the limited sparse subarray apertures. Moreover, the proposed coarray tensor completion algorithm presents the highest angular resolution among all evaluated methods. In partic-

ular, compared to the matrix-based methods, the proposed algorithm obtains the improvement from the virtual cubic array formulation by preserving the relevance among the virtual sensors. On the other hand, compared to the coarray tensor MUSIC method utilizing the continuous part of the virtual planar array  $\mathbb{U}$  only, the proposed algorithm demonstrates an enhanced resolution, which is benefited from the larger aperture of the filled virtual cubic array  $\mathbb{W}$ .

### D. Estimation accuracy comparison for coherent sources

Although far-field narrowband sources are assumed to be uncorrelated in our signal model, the proposed coarray tensor completion algorithm also works for coherent sources DOA estimation. In the last example, we evaluate the performance of the proposed algorithm for  $K = 2$  fully correlated sources with DOAs  $(\theta_1, \phi_1) = (21.6^\circ, 32.6^\circ)$  and  $(\theta_2, \phi_2) = (50.5^\circ, 65.5^\circ)$ . Due to the coherency between the coherent sources' signals, the second source signal  $s_2$  can be represented as  $s_2 = \beta s_1$ , where  $\beta \in \mathbb{C}$  is an attenuation factor. The proposed algorithm is compared to the spatial smoothing MUSIC method ('SS-MUSIC') [46] and the coarray ESPRIT method [17]. To be specific, the spatial smoothing MUSIC method incorporates the ideas of spatial smoothing and coprime subarray decomposition, while the coarray ESPRIT method applies spatial smoothing to the second-order coarray statistics for decorrelated DOA estimation. The RMSE of DOA estimation defined in (47) is used as the evaluation metric, where the real and imaginary parts of  $\beta$  are both randomly generated following the zero-mean unit-variance Gaussian distribution for each trial.

As shown in Fig. 9, the proposed coarray tensor completion algorithm outperforms both the spatial smoothing MUSIC and coarray ESPRIT methods for coherent

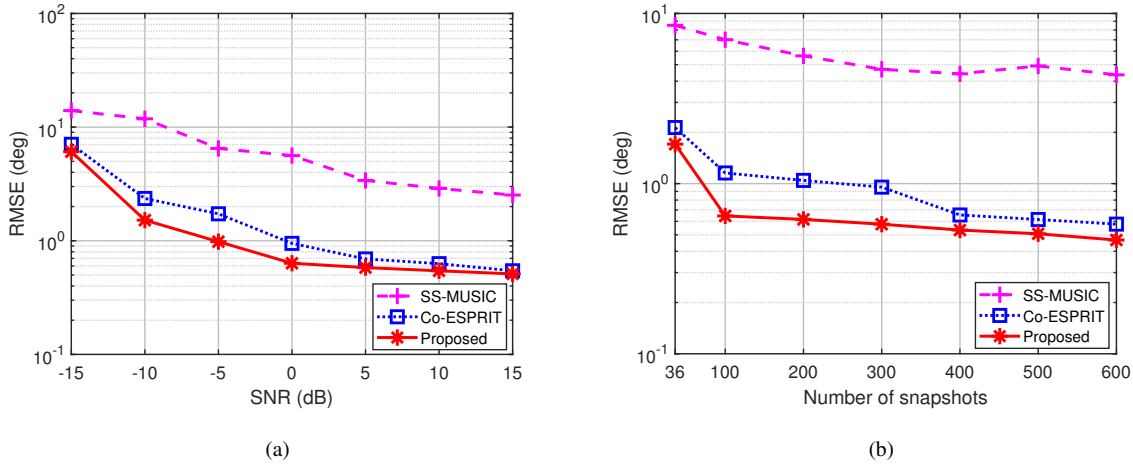


Fig. 9. Estimation accuracy comparison for coherent sources. (a) RMSE versus SNR. (b) RMSE versus the number of snapshots.

sources DOA estimation. This comes from the fact that the proposed algorithm takes full advantage of coarray information with tensorial optimization for multi-dimensional sub-Nyquist signals, leading to an enhanced source decorrelation capability.

## VI. Conclusion

In this paper, we proposed a coarray tensor completion algorithm for 2-D DOA estimation. The proposed algorithm makes full use of the discontinuous virtual array derived from the cross-correlation tensor statistics, and the corresponding equivalent second-order signals are represented by an incomplete coarray tensor. To impose an effective low-rank regularization on the coarray tensor, its whole missing slices are sufficiently dispersed under the principle of maximizing the DPR of missing elements. As such, the reformulated coarray tensor can be completed by solving a coarray tensor nuclear norm minimization problem via the ADMM. Meanwhile, the global convergence of the coarray tensor completion problem is theoretically proved. Then, the 2-D DOAs of sources are estimated in a closed-form manner by applying CPD to the completed coarray tensor corresponding to the filled virtual array. Simulation results corroborate the superior performance of the proposed algorithm in both estimation accuracy and resolution compared to competing methods.

The proposed algorithm can be extended to other parameter estimation scenarios with partially augmentable sparse arrays. For example, the slice-missing coarray tensor completion method can be applied to the sparse MIMO system for joint angle/frequency estimation with full utilization of multi-dimensional coarray statistics. Moreover, in imaging scenarios, the designed tensor segmentation and structured tensor formulation approaches can be adopted to restore images or accelerate imaging process.

## Appendix A

### ADMM implementation for coarray tensor completion

By introducing dual variables  $\mathcal{M}_j \in \mathbb{C}^{L_x L_y \times U_x U_y \times 2}$  of  $\bar{\mathcal{D}}$  with  $j \in \{1, 2, \dots, o(\bar{\mathcal{D}})\}$ , the augmented Lagrangian function of the formulated coarray tensor nuclear norm minimization problem (26) can be defined as

$$\begin{aligned} \mathcal{L}(\bar{\mathcal{D}}, \mathcal{Y}_1, \mathcal{Y}_2, \mathcal{Y}_3, \mathcal{M}_1, \mathcal{M}_2, \mathcal{M}_3) \\ = \|\bar{\mathcal{D}}\|_* + \langle \mathcal{Y}_j - \bar{\mathcal{D}}, \mathcal{M}_j \rangle + \frac{\rho}{2} \|\mathcal{Y}_j - \bar{\mathcal{D}}\|_F^2, \end{aligned} \quad (50)$$

where  $\rho > 0$  is the penalty constant. Based on the framework of ADMM,  $\bar{\mathcal{D}}$ ,  $\mathcal{Y}_j$  and  $\mathcal{M}_j$  at the  $(n_A + 1)$ -th iteration can be updated as

$$\begin{aligned} \mathcal{Y}_j^{(n_A+1)} &= \underset{\mathcal{Y}_j}{\operatorname{argmin}} \mathcal{L}(\bar{\mathcal{D}}^{(n_A)}, \mathcal{Y}_j, \mathcal{M}_j^{(n_A)}), \\ \bar{\mathcal{D}}^{(n_A+1)} &= \underset{\bar{\mathcal{D}}}{\operatorname{argmin}} \mathcal{L}(\bar{\mathcal{D}}, \mathcal{Y}_j^{(n_A+1)}, \mathcal{M}_j^{(n_A)}), \\ \mathcal{M}_j^{(n_A+1)} &= \mathcal{M}_j^{(n_A)} - \rho (\mathcal{Y}_j^{(n_A+1)} - \bar{\mathcal{D}}^{(n_A+1)}). \end{aligned} \quad (51)$$

The closed-form solution to  $\mathcal{Y}_j^{(n_A+1)}$  and  $\bar{\mathcal{D}}^{(n_A+1)}$  in (51) can be obtained as

$$\begin{aligned} \mathcal{Y}_j^{(n_A+1)} &= \operatorname{fold}_{(j)} \left( \Upsilon_{\frac{\alpha_j}{\rho}} \left( [\bar{\mathcal{D}}^{(n_A)}]_{(j)} + \frac{1}{\rho} [\mathcal{M}_j^{(n_A+1)}]_{(j)} \right) \right), \\ P_{\Omega}(\bar{\mathcal{D}}^{(n_A+1)}) &= P_{\Omega} \left( \frac{1}{o(\bar{\mathcal{D}})} \left( \sum_{j=1}^{o(\bar{\mathcal{D}})} \mathcal{Y}_j^{(n_A+1)} - \frac{1}{\rho} \mathcal{M}_j^{(n_A)} \right) \right), \\ P_{\bar{\Omega}}(\bar{\mathcal{D}}^{(n_A+1)}) &= P_{\bar{\Omega}}(\bar{\mathcal{D}}), \end{aligned} \quad (52)$$

where  $\operatorname{fold}_{(j)}(\cdot)$  represents the reversed operator of mode- $j$  tensor unfolding, and

$$\Upsilon_{\frac{\alpha_j}{\rho}}(\mathbf{X}) = \mathbf{F}_X \Sigma_X^{(\frac{\alpha_j}{\rho})} \mathbf{W}_X \quad (53)$$

denotes the shrinkage singular value decomposition operator on  $\mathbf{X} \in \mathbb{C}^{X_1 \times X_2}$ . Here,  $\mathbf{F}_X$ ,  $\mathbf{W}_X$  respectively

represent the left singular matrix and the right singular matrix of  $\mathbf{X}$ , and

$$\Sigma_X^{\left(\frac{\alpha_j}{\rho}\right)} = \text{diag}\left(\max\left(\eta_l - \frac{\alpha_j}{\rho}, 0\right)\right), \quad (54)$$

represents the singular value matrix, where  $\eta_l$  denotes the singular value of  $\mathbf{X}$ ,  $l \in \{1, 2, \dots, \min(X_1, X_2)\}$ ,  $\text{diag}(\cdot)$  forms a diagonal matrix from its arguments,  $\min(\cdot)$  and  $\max(\cdot)$  respectively represent the minimum and maximum operators.

Note that, the convergence of (51) can be accelerated by adaptively increasing the penalty constant  $\rho$  [31, 47]. In our simulations, we iteratively increase  $\rho$  by multiplying it with a positive constant  $u > 1$ , i.e.,  $\rho^{(n_A+1)} = u\rho^{(n_A)}$ .

## Appendix B

### CPD of the completed coarray tensor

The CPD of the completed coarray tensor  $\bar{\mathcal{D}}$  in (43) aims to approximate the outer product of its CP factors while minimizing the effect of the residual noise tensor  $\bar{\mathcal{B}}$ , which can be defined as the following least squares problem

$$\min_{\hat{\mathbf{V}}, \hat{\mathbf{G}}, \hat{\mathbf{H}}} \left\| \bar{\mathcal{D}} - \mathcal{J} \times_1 \hat{\mathbf{V}} \times_2 \hat{\mathbf{G}} \times_3 \hat{\mathbf{H}} \right\|_{\text{F}}^2. \quad (55)$$

Here,

$$\begin{aligned} \hat{\mathbf{V}} &= [\hat{\mathbf{v}}_1, \hat{\mathbf{v}}_2, \dots, \hat{\mathbf{v}}_K] \in \mathbb{C}^{L_x L_y \times K}, \\ \hat{\mathbf{G}} &= [\hat{\mathbf{g}}_1, \hat{\mathbf{g}}_2, \dots, \hat{\mathbf{g}}_K] \in \mathbb{C}^{U_x U_y \times K}, \\ \hat{\mathbf{H}} &= [\hat{\mathbf{h}}_1, \hat{\mathbf{h}}_2, \dots, \hat{\mathbf{h}}_K] \in \mathbb{C}^{2 \times K}, \end{aligned} \quad (56)$$

are the factor matrices of  $\bar{\mathcal{D}}$ , and  $\mathcal{J} \in \mathbb{C}^{K \times K \times K}$  is the signal power tensor with  $\sigma_{s_k}^2$  on its main diagonal.

The optimization problem (55) can be solved by the trilinear alternating least squares technique, which iteratively updates  $\hat{\mathbf{V}}$ ,  $\hat{\mathbf{G}}$  and  $\hat{\mathbf{H}}$  as

$$\begin{aligned} \hat{\mathbf{V}} &= \underset{\hat{\mathbf{V}}}{\text{argmin}} \left\| [\bar{\mathcal{D}}]_{(1)} - \hat{\mathbf{V}} (\hat{\mathbf{H}} \odot \hat{\mathbf{G}})^{\text{T}} \right\|_{\text{F}}^2, \\ \hat{\mathbf{G}} &= \underset{\hat{\mathbf{G}}}{\text{argmin}} \left\| [\bar{\mathcal{D}}]_{(2)} - \hat{\mathbf{G}} (\hat{\mathbf{H}} \odot \hat{\mathbf{V}})^{\text{T}} \right\|_{\text{F}}^2, \\ \hat{\mathbf{H}} &= \underset{\hat{\mathbf{H}}}{\text{argmin}} \left\| [\bar{\mathcal{D}}]_{(3)} - \hat{\mathbf{H}} (\hat{\mathbf{G}} \odot \hat{\mathbf{V}})^{\text{T}} \right\|_{\text{F}}^2. \end{aligned} \quad (57)$$

For the  $(n_C + 1)$ -th iteration of CPD, the closed-form solution to the factor matrices of  $\bar{\mathcal{D}}$  can be obtained as

$$\begin{aligned} \hat{\mathbf{V}}^{(n_C+1)} &= [\bar{\mathcal{D}}]_{(1)} \left[ (\hat{\mathbf{H}}^{(n_C)} \odot \hat{\mathbf{G}}^{(n_C)})^{\text{T}} \right]^{\dagger}, \\ \hat{\mathbf{G}}^{(n_C+1)} &= [\bar{\mathcal{D}}]_{(2)} \left[ (\hat{\mathbf{H}}^{(n_C)} \odot \hat{\mathbf{V}}^{(n_C)})^{\text{T}} \right]^{\dagger}, \\ \hat{\mathbf{H}}^{(n_C+1)} &= [\bar{\mathcal{D}}]_{(3)} \left[ (\hat{\mathbf{G}}^{(n_C)} \odot \hat{\mathbf{V}}^{(n_C)})^{\text{T}} \right]^{\dagger}. \end{aligned} \quad (58)$$

The iterations in (57) repeat until the relative error of the decomposed coarray tensor between successive iterations is smaller than a convergence threshold  $\xi_{\text{CPD}}$ , and the three estimated factor matrices  $\hat{\mathbf{V}}$ ,  $\hat{\mathbf{G}}$  and  $\hat{\mathbf{H}}$  can be utilized for retrieving the azimuth and elevation angles as in (45).

The CPD of the completed coarray tensor  $\bar{\mathcal{D}}$  is essentially unique if

$$\kappa(\hat{\mathbf{V}}) + \kappa(\hat{\mathbf{G}}) + \kappa(\hat{\mathbf{H}}) \geq 2K + 2, \quad (59)$$

where  $\kappa(\cdot)$  denotes the Kruskal's rank of the factor matrix. By substituting  $\kappa(\hat{\mathbf{V}}) = \min(L_x L_y, K) = L_x L_y$ ,  $\kappa(\hat{\mathbf{G}}) = \min(U_x U_y, K) = U_x U_y$ , and  $\kappa(\hat{\mathbf{H}}) = \min(2, K) = 2$  into (59), we have

$$K \leq (L_x L_y + U_x U_y) / 2, \quad (60)$$

which provides the upper bound for the number of distinguishable sources. Note that, since the size of coarray sub-tensors  $(L_x, L_y)$  is optimized based on the principle of maximizing the DPR of missing elements in the coarray tensor, we aim to guarantee the best performance of coarray tensor completion instead of the maximum degrees-of-freedom. Hence, the upper bound of  $K$  in (60) is not the optimal result. In another work [27], we investigate the maximum degrees-of-freedom by devising a different coarray sub-tensor size optimization problem, which however, is out of scope of this paper.

## REFERENCES

- [1] H. Zheng, C. Zhou, A. L. F. de Almeida, Y. Gu, and Z. Shi  
DOA estimation via coarray tensor completion with missing slices  
In *Proc. IEEE Int. Conf. Acoust., Speech, Signal Process. (ICASSP)*, Singapore, May 2022, pp. 5053–5057.
- [2] H. L. Van Trees  
*Detection, Estimation, and Modulation Theory, Part IV: Optimum Array Processing*. New York, NY, USA: Wiley, 2002.
- [3] B. Liao  
Fast angle estimation for MIMO radar with nonorthogonal waveforms  
*IEEE Trans. Aerosp. Electron. Syst.*, vol. 54, no. 4, pp. 2091–2096, Aug. 2018.
- [4] C. Zhou, Y. Gu, Z. Shi, and Y. D. Zhang  
Off-grid direction-of-arrival estimation using coprime array interpolation  
*IEEE Signal Process. Lett.*, vol.25, no.11, pp. 1710–1714, Nov. 2018.
- [5] Z. Zhang, Z. Shi, and Y. Gu  
Ziv-Zakai bound for DOAs estimation  
*IEEE Trans. Signal Process.*, vol. 71, pp. 136–149, 2023.
- [6] V. S. Doan and D. S. Kim  
DOA estimation of multiple non-coherent and coherent signals using element transposition of covariance matrix  
*ICT Express*, vol. 6, no. 2, pp. 67–75, June 2020.
- [7] P. P. Vaidyanathan and P. Pal  
Sparse sensing with co-prime samplers and arrays  
*IEEE Trans. Signal Process.*, vol. 59, no. 2, pp. 573–586, Feb. 2011.
- [8] P. Pal and P. P. Vaidyanathan  
Nested arrays: A novel approach to array processing with enhanced degrees of freedom  
*IEEE Trans. Signal Process.*, vol. 58, no. 8, pp. 4167–4181, Aug. 2010.
- [9] S. Qin, Y. D. Zhang, and M. G. Amin  
Generalized coprime array configurations for direction-of-arrival estimation

- IEEE Trans. Signal Process.*, vol. 63, no. 6, pp. 1377–1390, Mar. 2015.
- [10] X. L. Tran, T. H. Nguyen, J. Vesely, F. Dvorak, V. M. Duong, and V. S. Doan  
Optimization of non-uniform planar antenna array topology in two-dimensional DOA estimation  
*Adv. Mil. Technol.*, vol. 15, no. 2, pp. 393–403, Nov. 2020.
- [11] X. Wu and W.-P. Zhu  
Single far-field or near-field source localization with sparse or uniform cross array  
*IEEE Trans. Veh. Technol.*, vol. 69, no. 8, pp. 9135–9139, Aug. 2020.
- [12] G. Qin, M. G. Amin, and Y. D. Zhang  
DOA estimation exploiting sparse array motions  
*IEEE Trans. Signal Process.*, vol. 67, no. 11, pp. 3013–3027, June 2019.
- [13] X. Zhang, Z. Zheng, W.-Q. Wang, and H. C. So  
DOA estimation of mixed circular and noncircular sources using nonuniform linear array  
*IEEE Trans. Aerosp. Electron. Syst.*, vol. 58, no. 6, pp. 5703–5710, Dec. 2022.
- [14] Z. Mao, S. Liu, Y. D. Zhang, L. Han, and Y. Huang  
Joint DoA-range estimation using space-frequency virtual difference coarray  
*IEEE Trans. Signal Process.*, vol. 70, pp. 2576–2592, May 2022.
- [15] P. Pal and P. P. Vaidyanathan  
Coprime sampling and the MUSIC algorithm  
*In Proc. IEEE Digit. Signal Process. Signal Process. Educ. Meeting*, Sedona, AZ, Jan. 2011, pp. 289–294.
- [16] C.-L. Liu and P. P. Vaidyanathan  
Remarks on the spatial smoothing step in coarray MUSIC  
*IEEE Signal Process. Lett.*, vol. 22, no. 9, pp. 1438–1442, Sept. 2015.
- [17] C. Zhou and J. Zhou  
Direction-of-arrival estimation with coarray ESPRIT for coprime array  
*Sensors*, vol. 17, no. 8, p. 1779, Aug. 2017.
- [18] Y. D. Zhang, M. G. Amin, and B. Himed  
Sparsity-based DOA estimation using co-prime arrays  
*In Proc. IEEE Int. Conf. Acoust., Speech, Signal Process. (ICASSP)*, Vancouver, Canada, May 2013, pp. 3967–3971.
- [19] C. Zhou, Y. Gu, Z. Shi, and M. Haardt  
Structured Nyquist correlation reconstruction for DOA estimation with sparse arrays  
*IEEE Trans. Signal Process.*, vol. 71, no. 21, pp. 101–114, Mar. 2023.
- [20] P. Comon, X. Luciani, and A. L. F. de Almeida  
Tensor decompositions, alternating least squares and other tales  
*J. Chemom.*, vol. 23, no. 7–8, pp. 393–405, Apr. 2009.
- [21] H. Chen, F. Ahmad, S. A. Vorobyov, and F. Porikli  
Tensor decompositions in wireless communications and MIMO radar  
*IEEE J. Sel. Topics Signal Process.*, vol. 15, no. 3, pp. 438–453, Apr. 2021.
- [22] F. Xu, M. W. Morency, and S. A. Vorobyov  
DOA estimation for transmit beamspace MIMO radar via tensor decomposition with Vandermonde factor matrix  
*IEEE Trans. Signal Process.*, vol. 70, pp. 2901–2917, May 2022.
- [23] H. Zheng, C. Zhou, Z. Shi, and Y. Gu  
Structured tensor reconstruction for coherent DOA estimation  
*IEEE Signal Process. Lett.*, vol. 29, pp. 1634–1638, July 2022.
- [24] S. Na, K. V. Mishra, Y. Liu, Y. C. Eldar, and X. Wang  
TenDSuR: Tensor-based 4D sub-Nyquist radar  
*IEEE Signal Process. Lett.*, vol. 26, no. 2, pp. 237–241, Feb. 2019.
- [25] J. Shi, F. Wen, and T. Liu  
Nested MIMO radar: Coarrays, tensor modeling, and angle estimation  
*IEEE Trans. Aerosp. Electron. Syst.*, vol. 57, no. 1, pp. 573–585, Feb. 2021.
- [26] H. Zheng, C. Zhou, Z. Shi, and A. L. F. de Almeida  
SubTTD: DOA estimation via sub-Nyquist tensor train decomposition  
*IEEE Signal Process. Lett.*, vol. 29, pp. 1978–1982, Aug. 2022.
- [27] H. Zheng, C. Zhou, Y. Gu, and Z. Shi  
Two-dimensional DOA estimation for coprime planar array: A coarray tensor-based solution  
*In Proc. IEEE Int. Conf. Acoust., Speech, Signal Process. (ICASSP)*, Barcelona, Spain, May 2020, pp. 4562–4566.
- [28] C.-L. Liu, P. P. Vaidyanathan, and P. Pal  
Coprime coarray interpolation for DOA estimation via nuclear norm minimization  
*In Proc. IEEE Int. Symp. Circuits Syst.*, Montréal, Canada, May 2016, pp. 2639–2642.
- [29] C. Zhou, Y. Gu, X. Fan, Z. Shi, G. Mao, and Y. D. Zhang  
Direction-of-arrival estimation for coprime array via virtual array interpolation  
*IEEE Trans. Signal Process.*, vol. 66, no. 22, pp. 5956–5971, Nov. 2018.
- [30] S. Grandy, B. Recht, and I. Yamada  
Tensor completion and low-n-rank tensor recovery via convex optimization  
*Inverse Prob.*, vol. 27, no. 2, p. 025010, Jan. 2011.
- [31] J. Liu, P. Musialski, P. Wonka, and J. Ye  
Tensor completion for estimating missing values in visual data  
*IEEE Trans. Pattern Anal. Mach. Intell.*, vol. 35, no. 1, pp. 208–220, Jan. 2013.
- [32] T. Yokota, B. Erem, S. Guler, S. K. Warfield, and H. Hontani  
Missing slice recovery for tensors using a low-rank model in embedded space  
*In Proc. IEEE Int. Conf. Computer Vision Pattern Recognit. (CVPR)*, Salt Lake City, UT, June 2018, pp. 8251–8259.
- [33] F. Sedighin, A. Cichocki, T. Yokota, and Q. Shi  
Matrix and tensor completion in multiway delay embedded space using tensor train, with application to signal reconstruction  
*IEEE Signal Process. Lett.*, vol. 27, pp. 810–814, Apr. 2020.
- [34] C. I. Kanatsoulis, X. Fu, N. D. Sidiropoulos, and M. Akçakaya  
Tensor completion from regular sub-Nyquist samples  
*IEEE Trans. Signal Process.*, vol. 68, pp. 1–16, 2020.
- [35] B. Recht, M. Fazel, and P. A. Parrilo  
Guaranteed minimum-rank solutions of linear matrix equations via nuclear norm minimization  
*SIAM Review*, vol. 52, no. 3, pp. 471–501, Aug. 2010.
- [36] Z. Lin, M. Chen, and Y. Ma  
*The Augmented Lagrange Multiplier Method for Exact Recovery of Corrupted Low-Rank Matrices*. Technical Report UILU-ENG-09-2215, UIUC, Nov. 2009.
- [37] M. Ding, T. Huang, X. Zhao, and T.-H. Ma

Tensor completion via nonconvex tensor ring rank minimization with guaranteed convergence

*Signal Process.*, vol. 194, p. 108425, May 2022.

- [38] M. Fazel, H. Hindi, and S. P. Boyd  
Log-det heuristic for matrix rank minimization with applications to Hankel and Euclidean distance matrices  
*In Proc. American Control Conf.*, Denver, CO, Nov. 2003, pp. 2156–2162.
- [39] Y.-D. Huang and M. Barkat  
Near-field multiple source localization by passive sensor array  
*IEEE Trans. Antennas Propag.*, vol. 39, no. 7, pp. 968–975, July 1991.
- [40] J. Shi, G. Hu, X. Zhang, F. Sun, and H. Zhou  
Sparsity-based two-dimensional DOA estimation for coprime array: From sum-difference coarray viewpoint  
*IEEE Trans. Signal Process.*, vol. 65, no. 21, pp. 5591–5604, Nov. 2017.
- [41] C.-L. Liu and P. P. Vaidyanathan  
Tensor MUSIC in multidimensional sparse arrays  
*In Proc. Asilomar Conf. Signals, Syst., Comput.*, Pacific Grove, CA, Nov. 2015, pp. 1783–1787.
- [42] J. He, Z. Zhang, C. Gu, T. Shu, and W. Yu  
Cumulant-based 2-D direction estimation using an acoustic vector sensor array  
*IEEE Trans. Aerosp. Electron. Syst.*, vol. 56, no. 2, pp. 956–971, Apr. 2020.
- [43] C. Zhou, Z. Shi, Y. Gu, and X. Shen  
DECOM: DOA estimation with combined MUSIC for coprime array  
*In Proc. Int. Conf. Wireless Commun. & Signal Process. (WCSP)*, Hangzhou, China, Oct. 2013, pp. 1–5.
- [44] C.-L. Liu and P. P. Vaidyanathan  
Cramér-Rao bounds for coprime and other sparse arrays, which find more sources than sensors  
*Digit. Signal Process.*, vol. 61, pp. 43–61, Feb. 2017.
- [45] M. Wang and A. Nehorai  
Coarrays, MUSIC, and the Cramér-Rao bound  
*IEEE Trans. Signal Process.*, vol. 65, no. 4, pp. 933–946, Feb. 2017.
- [46] H. Jiang, L. Li, M. Pu, H. Zhang, and X. Li  
The DOA estimation for a mixture of uncorrelated and coherent sources via decomposing the coprime array  
*Wirel. Commun. Mob. Comput.*, vol. 2022, p. 1961988, Nov. 2022.
- [47] K. Huang, N. D. Sidiropoulos, and A. P. Liavas  
A flexible and efficient algorithmic framework for constrained matrix and tensor factorization  
*IEEE Trans. Signal Process.*, vol. 64, no. 19, pp. 5052–5065, Oct. 2016.



**Hang Zheng** (Graduate Student Member, IEEE) received the B.E. degree in transportation engineering from Tongji University, Shanghai, China, in 2019. He is currently working toward the Ph.D. degree with the college of information science and electronic engineering, Zhejiang University, Hangzhou, China. He is also a visiting student at Aalto University, Espoo, Finland. His research interests include array signal processing, tensor signal processing, and machine learning. He was the recipient of the Best Paper Award from ISAP 2020 and ICAUS 2022.



**Zhiguo Shi** (Senior Member, IEEE) received the B.S. and Ph.D. degrees in electronic engineering from Zhejiang University, Hangzhou, China, in 2001 and 2006, respectively. Since 2006, he has been a Faculty Member with the College of Information Science and Electronic Engineering, Zhejiang University, where he is currently a Full Professor. From 2011 to 2013, he visited the Broadband Communications Research Group, University of Waterloo, Waterloo, ON, Canada. His research interests include array signal processing, localization, and internet-of-things.

Prof. Shi was the recipient of the 2019 IET Communications Premium Award, and coauthored a paper that received the 2021 IEEE Signal Processing Society Young Author Best Paper Award. He was also the recipient of the Best Paper Award from ISAP 2020, IEEE GLOBECOM 2019, IEEE WCNC 2017, IEEE/CIC ICC 2013, and IEEE WCNC 2013. He was the General Co-Chair of IEEE SAM 2020 and served as an Editor for the IEEE Network. He is currently serving as an Associate Editor for the IEEE Signal Processing Letters, IEEE Transactions on Vehicular Technology, IET Communications, and Journal of the Franklin Institute. He is an elected member of the Sensor Array and Multichannel (SAM) Technical Committee of the IEEE Signal Processing Society.



**Chengwei Zhou** (Member, IEEE) received the Ph.D. degree in electronic science and technology from Zhejiang University, Hangzhou, China, in 2018. He was a Visiting Researcher at University of Technology Sydney, Sydney, NSW, Australia, from April 2017 to October 2017. He served as a postdoctoral research fellow at the State Key Laboratory of Industrial Control Technology, the College of Control Science and Engineering, Zhejiang University, Hangzhou, China, from 2018 to 2020. Since June 2020, he has been a Research Associate Professor with the College of Information Science and Electronic Engineering, Zhejiang University, Hangzhou, China. His current research interests are in the areas of array signal processing, direction-of-arrival estimation, and adaptive beamforming.

Dr. Zhou currently serves as an Associate Editor for International Journal of Communication Systems, and an Editorial Board Member of Journal of Signal Processing (in Chinese). He was the recipient of the 2021 IEEE Signal Processing Society Young Author Best Paper Award, ISAP 2020 Best Paper Award, and 2019 IET Communications Premium Award.



**André L. F. de Almeida** (Senior Member, IEEE) is a Professor at the Teleinformatics Engineering Department of the Federal University of Ceara. He received a double Ph.D. degree in Sciences and Teleinformatics Engineering from the University of Nice, Sophia Antipolis, France, and the Federal University of Ceara, Fortaleza, Brazil, in 2007. From 2007 to 2008, he held a one-year teaching position at the University of Nice Sophia Antipolis, France.

He was awarded multiple times visiting professor positions at the University of Nice Sophia Antipolis, France (2012, 2013, 2015, 2018, 2019).

Prof. Almeida served as an Associate Editor for several journals, such as the IEEE Transactions on Signal Processing (2012-2014 and 2014-2016), IEEE Signal Processing Letters (2016-2018 and 2018-2020), and IEEE Transactions on Vehicular Technology (2020-2022). He currently serves as a Senior Area Editor for the IEEE Signal Processing Letters. He has also served as Guest Editor for the EURASIP Journal on Advances in Signal Processing (2014, 2022), and Wireless

Communications and Mobile Computing (2018, 2019). Prof. Almeida is an elected member of the IEEE Signal Processing Society (SPS) Signal Processing Theory and Methods (SPTM) Technical Committee (2022-2024), and an elected member of the EURASIP Signal Processing for Multi-Sensor Systems Technical Area Committee (SPMuS TAC) (2016-2018 and 2019-2022). He is vice-chair of the EURASIP SPMuS TAC (2022-2023). He served as an elected member of the IEEE SPS Sensor Array and Multichannel (SAM) Technical Committee (2015-2018 and 2018-2021). He also served as an associate member of the Big Data Special Interest Group (SIG) of the IEEE SPS (2015-2018). Prof. Almeida currently serves as an IEEE SPS Regional Director-at-Large for Regions 7 & 9 (2022-2023). He was involved in the organization and chairing of several IEEE SPS conferences. In particular, he was a General Co-Chair of the 2017 IEEE International Workshop on Computational Advances in Multi-Sensor Adaptive Processing (CAMSAP'2017), Technical Co-Chair of the IEEE GlobalSIP'2018 and IEEE GlobalSIP'2019 Symposia on Tensor Methods for Signal Processing and Machine Learning, Technical Co-Chair of the 11th IEEE Sensor Array and Multichannel Signal Processing Workshop (SAM'2020) and is the General Co-Chair of the IEEE CAMSAP'2023, Costa Rica. He is a level-1D research fellow of the CNPq (the Brazilian National Council for Scientific and Technological Development). In 2018, he was elected an Affiliate Member of the Brazilian Academy of Sciences. He is a co-recipient of the 2018 IET Communications Premium Award (2018), Best Paper Award at the 19th IEEE International Conference on OFDM and Frequency Domain Techniques (2016), Best Paper Award at the XXXVIII Brazilian Symposium of Telecommunications and Signal Processing (2020), and the 2022 IET Signal Processing Premium Best Paper Award (2022). He has published over 200 papers in journals and conferences, 6 book chapters, and is co-inventor of 5 international patents. He has coordinated internationally funded research projects in mobile wireless communications, massive MIMO systems, array signal processing, and 5G networks. His research interests lie in signal processing for communications and sensor array and multichannel processing, including topics such as channel estimation and equalization, multi-antenna systems, blind and semi-blind signal processing, and direction of arrival estimation. An important part of his research has been dedicated to multilinear algebra and tensor decompositions with applications to communication systems and signal processing.